

7SM

The Earth's Energy Budget, Climate Feedbacks and Climate Sensitivity Supplementary Material

Lead Authors:

Chris Smith (United Kingdom), Zebedee R. J. Nicholls (Australia), Kyle Armour (United States of America), William Collins (United Kingdom), Piers Forster (United Kingdom), Malte Meinshausen (Australia/Germany), Matthew D. Palmer (United Kingdom), Masahiro Watanabe (Japan)

Contributing Authors:

Thomas Gasser (Austria/France), Nicholas Leach (United Kingdom), Yann Quilcaille (Switzerland/France), Marit Sandstad (Norway), Mark Zelinka (United States of America)

This supplementary material should be cited as:

Smith, C., Z.R.J. Nicholls, K. Armour, W. Collins, P. Forster, M. Meinshausen, M.D. Palmer, and M. Watanabe, 2021: The Earth's Energy Budget, Climate Feedbacks, and Climate Sensitivity Supplementary Material. In *Climate Change 2021: The Physical Science Basis. Contribution of Working Group I to the Sixth Assessment Report of the Intergovernmental Panel on Climate Change* [Masson-Delmotte, V., P. Zhai, A. Pirani, S.L. Connors, C. Péan, S. Berger, N. Caud, Y. Chen, L. Goldfarb, M.I. Gomis, M. Huang, K. Leitzell, E. Lonnoy, J.B.R. Matthews, T.K. Maycock, T. Waterfield, O. Yelekçi, R. Yu, and B. Zhou (eds.)]. Available from <https://www.ipcc.ch/>.

Table of Contents

7.SM.1 Effective Radiative Forcing	3
7.SM.1.1 Simplified Expressions for Greenhouse Gases	3
7.SM.1.2 Effective Radiative Forcing from a Doubling of CO ₂	3
7.SM.1.3 Historical (1750–2019) Effective Radiative Forcing Time Series	4
7.SM.1.4 SSP and RCP Effective Radiative Forcing Time Series	6
7.SM.2 Two-Layer Energy Balance Model for Climate Emulation	9
7.SM.2.1 Emulator Definition	9
7.SM.2.2 Constrained Emulator Ensemble	9
7.SM.2.3 Supporting Information for Figures 7.7 and 7.8	10
7.SM.2.4 Supporting information for Figure SPM.4b	10
7.SM.3 Performance of Emulators Compared to Key Physical Climate Assessments	10
7.SM.4 Equilibrium Climate Sensitivity and Transient Climate Response from CMIP6 Models	12
7.SM.5 Climate Metrics	15
7.SM.5.1 Definitions of Climate Metrics	15
7.SM.5.2 Impulse-Response Functions for GTP and Chapter 6 Calculations	15
7.SM.6 Tables of Greenhouse Gas Lifetimes, Radiative Efficiencies and Metrics	16
7.SM.7 Data Table	29
References	33

7.SM.1 Effective Radiative Forcing

7.SM.1.1 Simplified Expressions for Greenhouse Gases

In Section 7.3.2 and Table 7.5, simplified expressions for the stratospheric-temperature-adjusted radiative forcing (SARF) are used to convert greenhouse gas (GHG) concentrations to radiative forcing. The AR5 (Myhre et al., 2013b) used relationships first introduced in Myhre et al. (1998), providing a logarithmic dependence of carbon dioxide (CO_2) SARF on CO_2 concentrations, and square-root dependencies of methane (CH_4) and nitrous oxide (N_2O) SARF on CH_4 and N_2O concentrations. The CH_4 and N_2O relationships accounted for band overlaps between these gases. These simplified expressions for SARF were revised in Etminan et al. (2016) using updated spectroscopic data. The most notable changes were a substantial revision in the methane SARF of about +25% to account for previously neglected shortwave effects (Section 7.3.2.2) and inclusion of the mutual band overlap between carbon dioxide and nitrous oxide (Section 7.3.2.1). In Etminan et al. (2016), calculations from the Oslo line-by-line (LBL) radiative transfer model were conducted for 48 cases that co-varied concentrations of carbon dioxide, methane and nitrous oxide that spanned values from 180–2000 ppm CO_2 , 340–3500 ppb CH_4 and 200–525 ppb N_2O . These ranges were selected to cover the minimum observed from ice-core records during the Last Glacial Maximum (LGM) to the maximum projected in the RCP8.5 scenario in the future (Meinshausen et al., 2011b; Riahi et al., 2011). Simplified relationships linking concentrations of CO_2 , CH_4 and N_2O to the SARF from each gas, including overlaps, were provided from these 48 different cases that fit the original line-by-line results within a few percent.

A more accurate but complex functional fit was provided in Meinshausen et al. (2020) to the 48 Oslo LBL cases in Etminan et al. (2016). Two main advantages to the Meinshausen et al. (2020) fit are (i) the reduced error in the new fits to the original Oslo LBL results (maximum 0.11% for the CO_2 cases compared to 3.6% in Etminan et al. (2016)) and (ii) the extension of the valid range of the fits to CO_2 concentrations above 2000 ppm, which occurs in SSP5-8.5 in the future (though not in RCP8.5). One drawback to the Meinshausen et al. (2020) fit compared to the original Etminan et al. (2016) fit is that the former is defined with respect to 1750 greenhouse gas concentrations, and requires a recalculation of the coefficients to use baseline concentrations that are different from this, whereas the Etminan et al. (2016) fit is valid for any baseline concentration within their stated validity range (180–2000 ppm CO_2 , 340–3500 ppb CH_4 , 200–525 ppb N_2O). In general, AR6 and Chapter 7 in particular reports SARF and effective radiative forcing (ERF) relative to a 1750 baseline, negating this possible drawback, and so the Meinshausen et al. (2020) relationships are used for computing SARF and ERF throughout Chapter 7 and in Annex III. The relationships converting concentrations to SARF are shown in Table 7.SM.1. For halogenated greenhouse gases with concentrations in the ppt range, SARF remains a linear function of concentrations, as in AR5.

7.SM.1.2 Effective Radiative Forcing from a Doubling of CO_2

In Section 7.3.2.1, the ERF from a doubling of CO_2 ($\Delta F_{2\times\text{CO}_2} = 3.93 \text{ W m}^{-2}$) is defined relative to 1750 concentrations of CO_2 assessed in Chapter 2 ($C_0 = 278.3 \text{ ppm}$) and N_2O ($N_0 = 270.1 \text{ ppb}$) using the Meinshausen et al. (2020) fits (Table 7.SM.1) to calculate SARF of 3.75 W m^{-2} and then adding an additional 5% for tropospheric adjustments (Section 7.3.2.1, Table 7.3). Using the

Table 7.SM.1 | Simplified expressions to compute radiative forcing (RF) from concentrations of greenhouse gases (Myhre et al., 1998; Meinshausen et al., 2020). C , N and M refer to concentrations of CO_2 in ppm, N_2O in ppb and CH_4 in ppb, respectively.

Gas	Radiative Forcing (SARF) Simplified Expression	Coefficients
CO_2	$C_{\alpha_{\max}} = C_0 - \frac{b_1}{2a_1}$ $\alpha' = \begin{cases} d_1 - \frac{b_1^2}{4a_1}, & C > C_{\alpha_{\max}} \\ d_1 + a_1(C - C_0)^2 + b_1(C - C_0), & C_0 < C < C_{\alpha_{\max}} \\ d_1, & C < C_0 \end{cases}$	$a_1 = -2.4785 \times 10^{-7} \text{ W m}^{-2} \text{ ppm}^{-2}$ $b_1 = 7.5906 \times 10^{-4} \text{ W m}^{-2} \text{ ppm}^{-1}$ $c_1 = -2.1492 \times 10^{-3} \text{ W m}^{-2} \text{ ppb}^{-1/2}$ $d_1 = 5.2488 \text{ W m}^{-2}$ $C_0 = 277.15 \text{ ppm}$
N_2O	$\text{SARF}_{\text{N}_2\text{O}} = (a_2\sqrt{C} + b_2\sqrt{N} + c_2\sqrt{M} + d_2)(\sqrt{N} - \sqrt{N_0})$	$a_2 = -3.4197 \times 10^{-4} \text{ W m}^{-2} \text{ ppm}^{-1/2} \text{ ppb}^{-1/2}$ $b_2 = 2.5455 \times 10^{-4} \text{ W m}^{-2} \text{ ppb}^{-1}$ $c_2 = -2.4357 \times 10^{-4} \text{ W m}^{-2} \text{ ppb}^{-1}$ $d_2 = 0.12173 \text{ W m}^{-2} \text{ ppb}^{-1/2}$ $N_0 = 273.87 \text{ ppb}$
CH_4	$\text{SARF}_{\text{CH}_4} = (a_3\sqrt{M} + b_3\sqrt{N} + d_3)(\sqrt{M} - \sqrt{M_0})$	$a_3 = -8.9603 \times 10^{-5} \text{ W m}^{-2} \text{ ppb}^{-1}$ $b_3 = -1.2462 \times 10^{-4} \text{ W m}^{-2} \text{ ppb}^{-1}$ $d_3 = 0.045194 \text{ W m}^{-2} \text{ ppb}^{-1/2}$ $M_0 = 731.41 \text{ ppb}$
Halogenated Compounds and Other Minor GHGs	$\text{SARF}_X = e_X(X - X_0)$	X and X_0 in ppb e_X is radiative efficiency ($\text{W m}^{-2} \text{ ppb}^{-1}$) (Table 7.SM.7)

Etminan et al. (2016) fits with the same baseline concentrations ($C_0 = 278.3 \text{ ppm}$, $N_0 = 270.1 \text{ ppb}$) results in a SARF of 3.80 W m^{-2} and an ERF of 3.99 W m^{-2} (Table 7.SM.2). The simplified expressions are used as no specific line-by-line experiment was performed for a doubling of CO_2 from about 1750 concentrations in Etminan et al. (2016).

Alongside the choice of simplified expression, the baseline CO_2 and N_2O concentrations also have an impact on the SARF and ERF from a doubling of CO_2 (Table 7.SM.2). Using 1850 CE baselines results in ERF values that are close, but not exactly the same, as using 1750 CE baselines (Table 7.SM.2). Using a present-day baseline results in estimates of SARF and ERF from a doubling of CO_2 that are about 1% greater than the 1750 or 1850 values (Table 7.SM.2). The 1850 baseline is significant as it is the reference pre-industrial state for CMIP6 experiments, including the *abrupt4xCO₂* and *1pctCO₂* experiments used to estimate ECS and TCR from climate models. It should be noted that the *1pctCO₂* experiment design relies on a logarithmic increase in CO_2 SARF with concentration to estimate TCR (Gregory et al., 2015), and both the Etminan et al. (2016) and Meinshausen et al. (2020) SARF formulas are super-logarithmic with increasing CO_2 concentrations.

7.SM.1.3 Historical (1750–2019) Effective Radiative Forcing Time Series

7.SM.1.3.1 Best Estimate Historical Time Series

The historical ERF time series describes how the best estimates of changes in climate drivers translates to ERF for 1750 to 2019. The time evolution of ERF is reported separately for CO_2 , CH_4 , N_2O , other well-mixed greenhouse gases (WMGHGs), ozone, stratospheric water vapour from methane oxidation, contrails and aviation-induced cirrus, aerosol–radiation interactions, aerosol–cloud interactions, light-absorbing particles on snow and ice, land-use change, volcanic and solar. The contributions from 49 halogenated GHGs comprising the ‘other well-mixed greenhouse gases’ category are further reported individually. Data is published in Annex III.

For CO_2 , CH_4 and N_2O , the SARFs are calculated using time-dependent best-estimate concentrations of these gases from Chapter 2 using the formulae in Table 7.SM.1 and using concentrations from Chapter 2 in 1750 as baselines ($C_0 = 278.3 \text{ ppm}$, $N_0 = 270.1 \text{ ppb}$, $M_0 = 729.2 \text{ ppb}$). Tropospheric adjustments of +5% for CO_2 , -14% for CH_4 and +7 % for N_2O are then added to these SARF values to produce ERF (Section 7.3.2). For 49 halogenated greenhouse gases, concentration changes since 1750 are used combined with radiative efficiencies detailed in Table 7.SM.7 to derive SARF (Table 7.SM.1). Accounting for tropospheric adjustments adds +13% and +12% to CFC-11 and CFC-12 respectively when moving from SARF to ERF. No tropospheric adjustments are assumed for other halogenated species (Section 7.3.2.4).

For historical ozone forcing, the time series from 1750 to 2020 from Skeie et al. (2020) is adopted, using the multi-model mean ERF from six independent Earth system and chemistry-climate models (BCC-ESM1, CESM2-WACCM6, GFDL-ESM4, GISS-E2-1-H, MRI-ESM2-0 and Oslo-CTM3) that used CMIP6 precursor emissions and interactively calculated ozone burdens using full stratospheric and tropospheric chemistry schemes. From the original 12 models reporting results in Skeie et al. (2020), CNRM-CM6, CNRM-ESM2-1 and E3SM1-0 were excluded as they do not include full stratospheric and tropospheric chemistry, only the first out of the similar models CESM2-WACCM6 and CESM2-CAM6 were used, the input4MIPs forcing estimate (Checa-Garcia et al., 2018) was excluded as it did not use CMIP6 precursor emissions, and UKESM-1-0-LL was excluded for having implausible time evolutions of stratospheric ozone that resulted in negative total ozone ERF estimates for 2010 relative to 1850. The extrapolations for the 1750–1850 and 2010–2020 periods (run beyond 2014 using SSP2-4.5) came from a single model (Oslo-CTM3) and results were used up to and including 2019. Stratospheric water vapour from methane oxidation is treated as scaling linearly with the methane ERF and scaled to the 1750–2019 assessment of 0.05 W m^{-2} (Section 7.3.2.6).

Several forcing categories (contrails and aviation-induced cirrus, aerosols and black carbon on snow) are derived from global annual emissions totals of short-lived climate forcers. For the best estimate

Table 7.SM.2 | Computed values of the SARF of a doubling of CO_2 using the relationships in Etminan et al. (2016) and Meinshausen et al. (2020), and the ERF from a doubling of CO_2 (assessed to be SARF + 5% in Section 7.3.2.1), from different baseline concentrations of CO_2 and N_2O , and compared to SARF in AR5.

CO_2 Concentration (ppm)	N_2O Concentration (ppb)	SARF $2 \times \text{CO}_2$ AR5 Myhre et al. (2013b)	SARF $2 \times \text{CO}_2$ Etminan et al. (2016)	ERF $2 \times \text{CO}_2$ Etminan et al. (2016)	SARF $2 \times \text{CO}_2$ Meinshausen et al. (2020)	ERF $2 \times \text{CO}_2$ Meinshausen et al. (2020)	Baseline Year for GHG Concentrations
278.3	270.1	3.71	3.802	3.992	3.747	3.934	1750 (Chapter 2 assessment)
277.15	273.87		3.801	3.991	3.746	3.933	1750 (Meinshausen et al., 2020)
284.32	273.02		3.804	3.994	3.749	3.937	1850 used in CMIP6 model integrations (Meinshausen et al., 2017)
389	323		3.837	4.029	3.790	3.980	2011 (Etminan et al., 2016)
409.85	332.09		3.844	4.036	3.798	3.988	2019 (Chapter 2 assessment)

of historical emissions from 1750 to 2019, the 11 September 2020 version of the Community Emissions Data System (CEDS) is used (Hoesly et al., 2018), obtained from <https://doi.org/10.5281/zenodo.4025316>. CEDS provides emissions of black carbon (BC), organic carbon (OC), sulphur dioxide (SO_2), ammonia (NH_3), nitrogen oxides (NO_x), carbon monoxide (CO), and non-methane volatile organic compounds (NMVOC) from the fossil fuel, industrial and agricultural sectors. Biomass-burning emissions are used from the BB4CMIP dataset (also used for CMIP6 model integrations, from Van Marle et al., 2017), aggregated into global annual totals. The SSP2-4.5 scenario projection from BB4CMIP is used for 2015–2019.

ERF from contrails and aviation-induced cirrus uses global aviation NO_x emissions as a predictor of aviation activity following Smith et al. (2018a), and scaled to the 2018 ERF best estimate of 0.0574 W m^{-2} from Lee et al. (2021).

ERF from aerosol–radiation interactions (ERFari) was calculated by converting emissions of BC, OC, SO_2 (representing sulphate aerosol) and NH_3 (representing nitrate aerosol) to forcing using CMIP5-era AeroCom multi-model mean contributions for each species from Myhre et al. (2013a) and scaled to obtain the assessment of -0.3 W m^{-2} for ERFari which is applied to the 2005–2014 decade. ERFari was calculated using a simple linear relationship to emissions of BC, OC, SO_2 and NH_3 ($E_{\text{BC}}, E_{\text{OC}}, E_{\text{SO}_2}, E_{\text{NH}_3}$):

$$\text{ERFari} = \beta_{\text{BC}} E_{\text{BC}} + \beta_{\text{OC}} E_{\text{OC}} + \beta_{\text{SO}_2} E_{\text{SO}_2} + \beta_{\text{NH}_3} E_{\text{NH}_3} \quad (7.\text{SM}.1.1)$$

The β coefficients are selected to represent ERFari contributions of $+0.3 \text{ W m}^{-2}$ from black carbon, -0.4 W m^{-2} from sulphate, -0.09 W m^{-2} from organic carbon and -0.11 W m^{-2} from nitrate over the 2005–2014 decade, which translates to radiative efficiencies of $\beta_{\text{BC}} = 50.8 \text{ mW yr m}^{-2} \text{ MtC}^{-1}$, $\beta_{\text{OC}} = -6.21 \text{ mW yr m}^{-2} \text{ MtC}^{-1}$, $\beta_{\text{SO}_2} = -3.62 \text{ mW yr m}^{-2} \text{ MtSO}_2^{-1}$, and $\beta_{\text{NH}_3} = -2.08 \text{ mW yr m}^{-2} \text{ MtNH}_3^{-1}$. Section 7.SM.1.3.2 explains the rationale for choosing these coefficients.

ERF from aerosol–cloud interactions (ERFaci) is modelled as a logarithmic function of emissions of SO_2 , BC and OC following Smith et al. (2018a):

$$\text{ERFaci} = -\beta \ln(1 + E_{\text{SO}_2}/s_{\text{SO}_2} + (E_{\text{BC+OC}}/s_{\text{BC+OC}})) \quad (7.\text{SM}.1.2)$$

Equation (7.SM.1.2) is based on the offline model of Ghan et al. (2013) using a functional form developed by Stevens (2015) with the inclusion of a carbonaceous aerosol term than can influence ERFaci. Equation (7.SM.1.2) was tuned to 11 CMIP6 models that provided historical time-varying (1850–2014) ERFaci estimates and a parameter set of β , s_{SO_2} and s_{BC} was obtained for each CMIP6 model. The parameter tunings from these 11 models were used to generate distributions using kernel density estimates from which 100,000 sample members were drawn and 100,000 candidate ERFaci

time series were produced. The best-estimate ERFaci time series is taken from the median of this 100,000-member ensemble, and then scaled to the assessed ERFaci of -1.0 W m^{-2} for 1750 to 2005–2014.

ERF from light-absorbing particles on snow is linear with BC emissions and scaled to the 1750–2019 ERF assessment of 0.08 W m^{-2} .

ERF from land-use change is broken down into an albedo component and an irrigation component. The albedo component follows the historical ERF time series from Ghimire et al. (2014) from 1700 to 2005, and is extended forward to 2019 using cumulative land-use related CO_2 emissions from the SSP historical and SSP2-4.5 scenarios. This follows the treatment in Smith et al. (2018a) and assumes that land-use related CO_2 is closely related to deforestation and albedo change. The 1750–2019 assessment of -0.15 W m^{-2} is then applied to the time series. The ERF from irrigation, assessed to be -0.05 W m^{-2} for 1750–2019 (Sherwood et al., 2018), scales with the albedo component.

All anthropogenic components of the ERF described above are expressed relative to a 1750 baseline.

Natural forcings comprise solar changes and volcanic eruptions (forcing from galactic cosmic rays is assessed to be negligible, Section 7.3.4.5). Volcanic ERF is derived from stratospheric aerosol optical depth (SAOD) using a conversion of $-20 \times \Delta \text{SAOD}$ (Section 7.3.4.6), or $\text{ERF} = -20 \times \text{SAOD} + 0.2582 \text{ W m}^{-2}$ using absolute SAOD where SAOD is nominally taken at 550 nm wavelength. The SAOD conversion to ERF is expressed as an anomaly in SAOD relative to the 500 BCE to 1749 CE mean, so that the mean volcanic ERF for 500 BCE to 1749 CE is zero. This is in order that the long-term mean GSAT change from pre-industrial volcanic forcing alone is zero, avoiding a spurious cooling effect when applying the volcanic time series from 1750 onwards to projections in a climate emulator (e.g., Section 7.SM.2). This convention means that volcanically quiescent years experience a volcanic ERF of up to $+0.2 \text{ W m}^{-2}$ (even volcanically quiescent years have some level of background stratospheric aerosol, so volcanic ERFs approaching the offset value of $+0.2582 \text{ W m}^{-2}$ are not seen). CMIP6 uses a similar prescription for volcanic forcing in ESMs, by applying a constant background climatology of SAOD for piControl and ScenarioMIP runs that is based on the historical (1850–2014) mean SAOD (Eyring et al., 2016).

The SAOD time series is derived from a composite of three datasets: eVolv v3 (Toohey and Sigl, 2017) for 500 BCE to 1900 CE, CMIP6 for 1850 to 1989, and GloSSAC v2 (Kovilakam et al., 2020) from 1979 to 2018. SAOD from GloSSAC v2 is reported at a wavelength of 525 nm and has been converted to 550 nm using an Ångström exponent of -2.33 (Kovilakam et al., 2020). The 2018 volcanic ERF is repeated for 2019. The 1850–1900 overlap is performed by linearly ramping down the eVolv v3 dataset and linearly ramping up the CMIP6 dataset. The CMIP6 and GloSSAC v2 data are ramped over the 1979–1989 period. In both cases the correspondences between overlapping periods is good.

Solar ERF is calculated using the change in total solar irradiance (TSI) where TSI is taken from the ^{14}C SATIRE-M reconstruction

from PMIP4 (Jungclaus et al., 2017) and converted to ERF using $\frac{1}{4} \times 0.71 \times 0.72 \times \Delta\text{TSI}$ (Section 7.3.4.4). The baseline for TSI is the mean TSI from 6754 BCE to 1744 CE, which encompasses complete solar cycles in the proxy reconstructions before 1750.

Aerosols and solar ERFs in 2019 both differ from the headline assessments given in Sections 7.3.3 and 7.3.4.4 respectively. For aerosols, the assessment in Section 7.3.3 of $-1.3 \pm 0.7 \text{ W m}^{-2}$ is valid for 1750 to about 2014, as less evidence is available for trends in how aerosol forcing has evolved in more recent years. The emissions-based time series provides a best-estimate aerosol ERF for 1750–2019 of -1.06 W m^{-2} , less negative than the 1750–2014 assessment, owing to a recent decline in precursor emissions since around 2005 from the CEDS dataset and supported by other studies (Paulot et al., 2018; Kanaya et al., 2020). For solar ERF, the Chapter 7 assessment of $+0.01 \pm 0.07 \text{ W m}^{-2}$ is for the 6754 BCE to 1744 CE pre-industrial period to the 2009–2019 solar cycle. The single year 2019, corresponding to a solar minimum, has a solar ERF of -0.02 W m^{-2} relative to this pre-industrial baseline.

7.SM.1.3.2 Uncertainties in the Historical Best-Estimate Time Series

The uncertainty in the historical ERF time series was generated with a 100,000-member Monte Carlo ensemble. The forcing components where uncertainty ranges are assumed to be symmetric and Gaussian in their assessments in Section 7.3 have a scale factor drawn from a Gaussian distribution with mean of unity and 5–95% uncertainty range determined as a fraction of the best-estimate ERF. The forcing components with symmetric uncertainty ranges are CO₂ (fractional 5–95% uncertainty 0.12 of the best estimate), CH₄ (0.20), N₂O (0.16), halogenated gases (0.19 on the basis that the majority are 'long-lived'), ozone (0.50), stratospheric water vapour (1.00), land-use change (0.50) and volcanic (0.25). Contrails (and aviation-induced cirrus) and light-absorbing particles on snow and ice have asymmetric uncertainty ranges and the fractional uncertainty was determined by considering ranges below and above the best estimate separately, by dividing the 5th percentile by the best estimate to derive the lower uncertainty range and the 95th percentile by the best estimate to determine the upper range, treating them as two halves of a Gaussian distribution. In each ensemble member the sampled uncertainty scale factor for each component of the forcing is applied to the whole time series.

For aerosols, the ERFari and ERFaci are treated independently. ERFari uncertainty is developed by sampling the radiative efficiency coefficients β_{BC} , β_{OC} , β_{SO_2} and β_{NH_3} in Equation (7.SM.1.1) as Gaussian distributions with 5–95%-range uncertainties of 0.67, 0.78, 0.50 and 0.44, yielding contributions to ERFari of $+0.3 \pm 0.2 \text{ W m}^{-2}$ for BC, $-0.4 \pm 0.2 \text{ W m}^{-2}$ for sulphate, $-0.09 \pm 0.07 \text{ W m}^{-2}$ for OC and $-0.11 \pm 0.05 \text{ W m}^{-2}$ for nitrate for the 2005–2014 mean with respect to 1750. Each precursor species is sampled independently and the historical emissions from the CEDS database are used to generate the time series of ERFari. These forcing contributions are based on modelling results from Myhre et al. (2013a), with scalings and uncertainty ranges for each component selected such that the total ERFari assessment of $-0.3 \pm 0.3 \text{ W m}^{-2}$ is preserved. These estimates

of per-species ERFari are independent of the headline assessments in Chapter 6, and differ particularly for BC (Section 6.4.2) where total BC ERFari is assessed to be $+0.145 \text{ W m}^{-2}$. The emulators in Chapter 7 are run with more positive ERF values for BC and more negative values for OC, SO₂ and NH₃ to preserve the assessed uncertainty range for total ERFari while maintaining a Gaussian uncertainty distribution for the forcing contribution from each species. As many aerosol precursors are co-emitted, the stronger best-estimate contributions per species used here offset each other and the time evolution and present-day values of total ERFari are broadly consistent between Chapter 6 and Chapter 7. It should be re-iterated here that the Chapter 7 values are not per-species assessments of ERFari and are used for the calibration and projection of climate in emulators. For ERFaci, the 100,000 generated time series described in Section 7.SM.1.3 are used with one additional step to scale each ERFaci candidate time series to a 2005–2014 mean ERFaci of $-1.0 \pm 0.7 \text{ W m}^{-2}$ with respect to 1750. This effectively rescales the β coefficients in each ensemble member in Equation (7.SM.1.2).

The 5–95% range of anthropogenic ERF of $1.96\text{--}3.48 \text{ W m}^{-2}$ (Table 7.8) for 1750–2019 is determined from the 5th and 95th percentiles of the year-2019 anthropogenic ERF in this 100,000-member ensemble.

For solar forcing, a 0.50 fractional uncertainty was applied to the amplitude of the solar cycle, and a linear 1750 to 2019 trend of $\pm 0.07 \text{ W m}^{-2}$ (5–95%) range was added to this to represent the uncertainty in the change in the underlying solar forcing (Section 7.3.4.4).

7.SM.1.4 SSP and RCP Effective Radiative Forcing Time Series

A similar method to the process described in Section 7.SM.1.3 is used to derive the ERF time series in RCP and SSP scenarios to 2500 (Chapters 6 and 9, Figure 4.35 and Annex III). From 1750 to 2014 the best estimate and uncertainty SSP projections ERF time series and the historical ERF time series described are identical. The SSPs diverge from each other, and from the historical best estimate, in 2015. For SSPs, the set of eight Tier 1 and Tier 2 scenarios defined by ScenarioMIP are assessed (SSP1-1.9, SSP1-2.6, SSP4-3.4, SSP5-3.4-over, SSP2-4.5, SSP4-6.0, SSP3-7.0 and SSP5-8.5). In addition two variants of SSP3-7.0 used primarily by AerChemMIP are presented: one where short-lived climate forcers are set to emissions factors consistent with strong air-quality controls that are broadly consistent with SSP1-levels of mitigation, SSP3-7.0-lowNTCF (Collins et al., 2017), plus a further variant of SSP3-7.0-lowNTCF that also takes into account methane mitigation alongside other short-lived forcers, SSP3-7.0-lowNTCFCH4 (Allen et al., 2021).

For 2015 to 2020, a linear transition between the concentrations of well-mixed greenhouse gases provided by Chapter 2 and the SSP greenhouse gas concentrations from Meinshausen et al. (2020) is performed. From 2020 onwards concentration projections from Meinshausen et al. (2020) are used. The correspondence between the Chapter 2 assessed time series and Meinshausen et al. (2017) dataset used for the CMIP6 historical experiment is good, with a maximum

difference of 0.6% from 1850 to 2014 for the main three greenhouse gases and 1.4% for N₂O in 1750 (the slight 1750 concentration differences affects the 2 × CO₂ forcing in the third decimal place; see Table 7.SM.2).

For purely emissions-based forcing estimates (aerosols, contrails and aviation-induced cirrus, and black carbon on snow), a similar five-year transition between 2015 and 2020 is performed for fossil fuel, industrial and agricultural emissions. The best-estimate historical emissions to 2019 are provided in the 11 September 2020 version of the CEDS database (<https://doi.org/10.5281/zenodo.4025316>) and the SSP scenario projections used v5.1 of the RCMIP dataset (obtained from <https://doi.org/10.5281/zenodo.4589756>; Nicholls et al., 2020) that provides consolidated regional and sectoral annual emissions totals from the CMIP6 SSP emissions datasets (Velders et al., 2015; Gidden et al., 2019; Meinshausen et al., 2020). Biomass-burning emissions are used from the SSP emissions projections from Van Marle et al. (2017). The same parameter sets from the historical ERF estimate and 100,000-member Monte Carlo ensemble are used to derive the future ERFs from aerosols, contrails (and aviation-induced cirrus) and black carbon on snow, using the SSP-emissions projections.

Future ozone forcing for SSP projections differs from the historical treatment and is based on emissions of short-lived forcers and concentrations of ozone-depleting greenhouse gases (Section 6.4). To generate the best-estimate projection, the historical time series in Skeie et al. (2020) is matched to emissions-driven estimates of ozone ERF from AerChemMIP models (Thornhill et al., 2021b), displayed in Table 7.SM.3 that sums to +0.37 W m⁻² for 1850 to 2014. There is a temperature-dependent feedback on ozone ERF of −0.037 W m⁻² °C⁻¹ for CMIP historical runs (this differs from the assessment in Section 6.4 of −0.064 W m⁻² °C⁻¹ which is based on *abrupt4xCO₂* experiments, as it includes the effects of the lightning NO_x and BVOC feedbacks that act to reduce the magnitude of the

temperature-ozone feedback; Thornhill et al., 2021a). As five of the six Earth system models run in Skeie et al. (2020) considered in the ERF-ozone assessment were CMIP historical runs (all except Oslo-CTM3) and simulated the increase in historical GSAT over time, they implicitly included this feedback and as such the −0.037 W m⁻² °C⁻¹ feedback is subtracted from the transient-ozone ERF in these five models, using GSAT time series assessed in Chapter 2, to produce a 'zero-feedback' estimate of ozone forcing from 1850 to 2014 of +0.47 W m⁻². To apply the emissions precursors to the overall time series, they are scaled by a factor of 1.27, derived from a ratio of the zero feedback estimate from Skeie et al. (2020) to the best estimate from the sum of precursors from Thornhill et al. (2021b) (0.47/0.37) to produce radiative efficiencies for each species (Table 7.SM.3).

The future ozone ERF is then derived as:

$$\begin{aligned} ERF_{O_3} = & \beta_{CH_4} \Delta C_{CH_4} + \beta_{N_2O} \Delta C_{N_2O} + \beta_{ODH} \Delta C_{ODH} + \beta_{CO} \Delta E_{CO} \\ & + \beta_{NMVOC} \Delta E_{NMVOC} + \beta_{NO_x} \Delta E_{NO_x} + f \cdot \Delta T \end{aligned} \quad (7.SM.1.3)$$

where C_{CH_4} and C_{N_2O} are concentrations of CH₄ and N₂O in ppb, C_{ODH} is the equivalent effective stratospheric chlorine from halogenated compounds expressed in ppt (Newman et al., 2007), and E_{CO} , E_{NMVOC} and E_{NO_x} are annual emissions in Mt yr⁻¹ (NO_x expressed in units of MtNO₂), $f = -0.037 \text{ W m}^{-2} \text{ }^{\circ}\text{C}^{-1}$ and ΔT represents GSAT anomaly. This configuration is run iteratively, with other best-estimate forcings, in the two-layer emulator (Section 7.SM.2) with the Section 7.5.5 best-estimate assessments of equilibrium climate sensitivity (ECS, 3.0°C) and transient climate response (TCR, 1.8°C) until convergence is achieved.

ERF from land use change scales with cumulative emissions of land-use-related CO₂ emissions following the end of the historical period.

Table 7.SM.3 | Effective radiative forcing from ozone precursors in AerChemMIP experiments (Thornhill et al., 2021b), and radiative efficiencies derived for emissions-based SSP pathways. The contributions for CO + NMVOC are not separated in Thornhill et al. (2021b) so the ratio of CO : NMVOC from CMIP5 ACCMIP experiments is used (Stevenson et al., 2013). Concentrations of ozone-depleting halocarbons (ODHs) are expressed in equivalent effective stratospheric chlorine in ppt.

Species	Contribution to Ozone ERF 1850–2014, W m ⁻² (Stevenson et al., 2013; Thornhill et al., 2021b)	Scale Factor to Reproduce 1850–2014 Ozone ERF in Skeie et al. (2020), After Subtracting Temperature Feedback	Radiative Efficiency for Ozone ERF
CH ₄	+0.14 ± 0.05	1.27	$\beta_{CH_4} = 0.175 \pm 0.062 \text{ mW m}^{-2} \text{ ppb}^{-1}$
N ₂ O	+0.03 ± 0.02		$\beta_{N_2O} = 0.710 \pm 0.062 \text{ mW m}^{-2} \text{ ppb}^{-1}$
Ozone-depleting Halocarbons (ODH)	−0.11 ± 0.10		$\beta_{ODH} = -0.125 \pm 0.113 \text{ mW m}^{-2} \text{ ppt}^{-1}$
CO	+0.07 ± 0.06		$\beta_{CO} = 0.155 \pm 0.131 \text{ mW m}^{-2} \text{ MtCO}^{-1} \text{ yr}$
NMVOC	+0.04 ± 0.04		$\beta_{NMVOC} = 0.329 \pm 0.328 \text{ mW m}^{-2} \text{ MtNMVOC}^{-1} \text{ yr}$
NO _x	+0.20 ± 0.11		$\beta_{NO_x} = 1.797 \pm 0.983 \text{ mW m}^{-2} \text{ MtNO}_2 \text{ yr}^{-1}$
Sum	+0.37 ± 0.18		+0.47 ± 0.24 W m ⁻² (total ozone ERF)

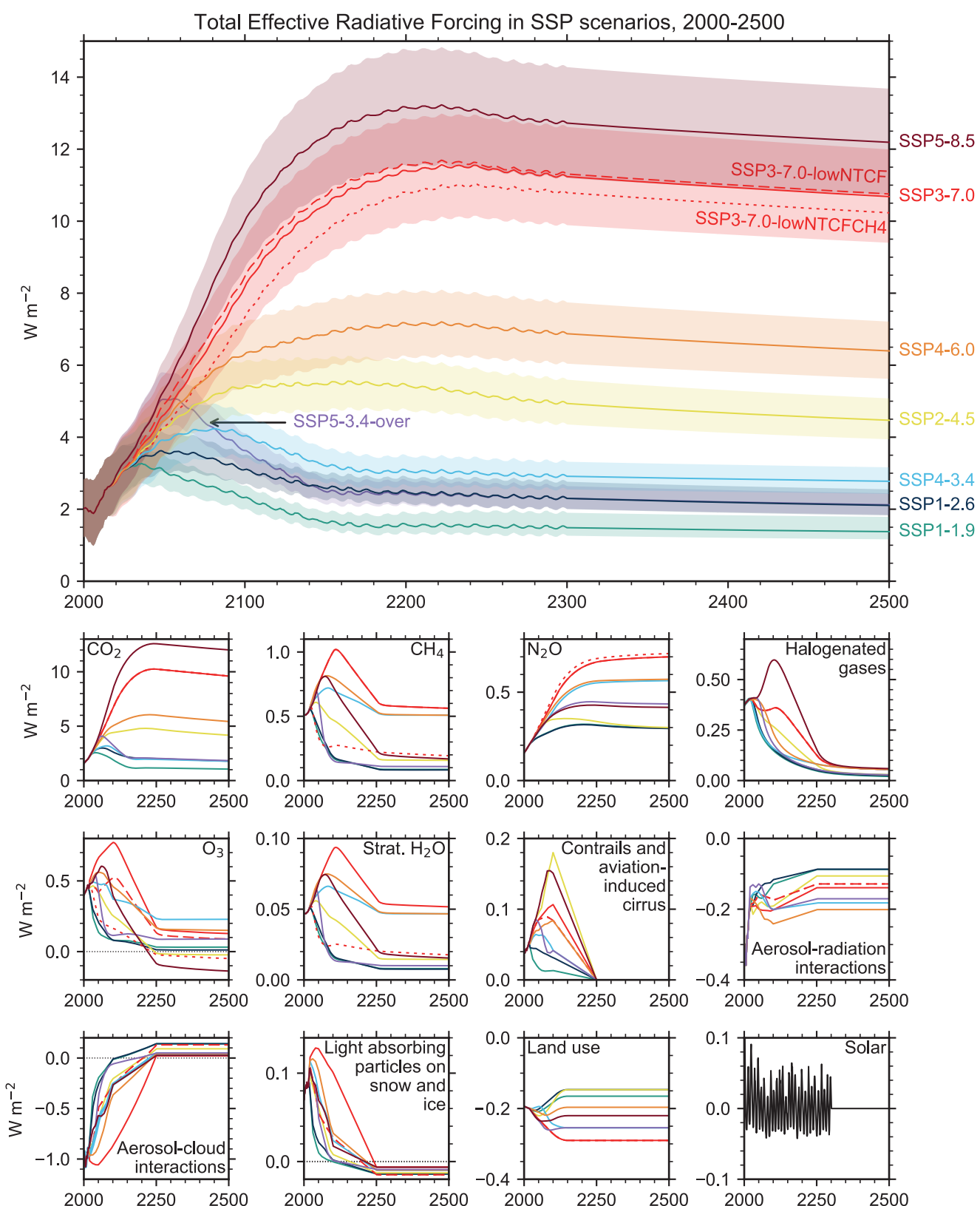


Figure 7.SM.1 | Total effective radiative forcing from SSP scenarios with respect to 1750 for 2000–2500 (top panel), showing best estimate and 5–95% uncertainty range (shaded regions). Uncertainty ranges are not shown for SSP3-7.0-lowNTCF and SSP3-7.0-NTCFCH4 for visual clarity. Bottom matrix shows the best-estimate ERF for each anthropogenic component and solar (volcanic ERF is zero beyond 2024).

Volcanic forcing is set to a ten-year linear ramp down to zero from 2014 to 2024, following the CMIP6 ScenarioMIP protocol (Eyring et al., 2016). Solar forcing uses the CMIP6 future TSI variation (Matthes et al., 2017) which provides projections to 2299, and is set to zero from 2300. For Figure 4.35 and Annex III, ERF time series for the RCP scenarios are produced using emissions and concentrations from Meinshausen et al. (2011b) using the same methods, present-day forcing best estimates, and uncertainty ranges described above, with the difference that scenarios start to diverge in 2005 and a 15-year ramp from 2005 to 2020 from historical emissions or concentrations to the future RCP projections is performed.

7.SM.2 Two-Layer Energy Balance Model for Climate Emulation

7.SM.2.1 Emulator Definition

The two-layer emulator is based on the following global mean equations:

$$\begin{aligned} C \frac{d}{dt} \Delta T &= \Delta F(t) + \alpha \Delta T - \varepsilon(\Delta T - \Delta T_d) \\ C_d \frac{d}{dt} \Delta T_d &= \gamma(\Delta T - \Delta T_d) \end{aligned} \quad (7.SM.2.1)$$

where ΔT ($^{\circ}\text{C}$) is the temperature of the surface layer (representing the surface components of the climate system), ΔT_d ($^{\circ}\text{C}$) is the temperature change in the deep ocean layer, C and C_d are the effective heat capacities for the surface and deep layers in $\text{W yr m}^{-2} ^{\circ}\text{C}^{-1}$, ε is the efficacy of the deep ocean heat uptake and γ is the heat transfer coefficient between the surface and deep layer ($\text{W m}^{-2} ^{\circ}\text{C}^{-1}$).

The analytical solution of Equation (7.SM.2.1) is expressed by a combination of fast and slow modes with the decay time scales of τ_f and τ_s . For a given value of ECS, TCR is obtained as:

$$\text{TCR} = \text{ECS} \left\{ 1 - \frac{1}{t} \left[\tau_f a_f \left(1 - e^{-\frac{t_0}{\tau_f}} \right) - \tau_s a_s \left(1 - e^{-\frac{t_0}{\tau_s}} \right) \right] \right\} \quad (7.SM.2.2)$$

The TCR is equal to ΔT at year $t = t_0 = 70$ in response to the forcing ΔF increasing at a rate of 1% per year, and all parameters (τ_f , τ_s , a_f , and a_s) can be calculated using C , C_d , γ , ε and the net feedback parameter α (the formulae are presented in Geoffroy et al., 2013a). As discussed in Jiménez-de-la-Cuesta and Mauritsen (2019), TCR can also be estimated directly from the two-layer model parameters as $\text{TCR} = \Delta F_{2\times\text{CO}_2}/(-\alpha + \kappa)$, where $\kappa = \varepsilon\gamma$.

The two-layer model can be calibrated to emulate the climate response of individual CMIP models (Geoffroy et al., 2013a, b) using abrupt4xCO₂ experiments. Calibrations are performed for 44 CMIP6 models resulting in parameter estimates (mean and standard deviation) of $C = 8.1 \pm 1.0 \text{ W yr m}^{-2} ^{\circ}\text{C}^{-1}$, $C_d = 110 \pm 63 \text{ W yr m}^{-2} ^{\circ}\text{C}^{-1}$, $\gamma = 0.62 \pm 0.13 \text{ W m}^{-2} ^{\circ}\text{C}^{-1}$, $\varepsilon = 1.34 \pm 0.41$, $\kappa = 0.84 \pm 0.38 \text{ W m}^{-2} ^{\circ}\text{C}^{-1}$.

Representative values from CMIP6 models in Equation (7.SM.2.2) are $\tau_f = 4.6 \text{ yr}$, $\tau_s = 333 \text{ yr}$, $a_f = 0.541$, $a_s = 0.459$.

7.SM.2.2 Constrained Emulator Ensemble

In several places in Working Group I (Figure SPM.4b, Chapters 1 and 9, Figures 7.7 and 7.8), a constrained ensemble of two-layer model projections is used. The starting point for this ensemble is a 1-million-member ensemble of emissions-driven historical runs using v1.6.2 of the FaIR emulator (Millar et al., 2017; Smith et al., 2018a). The temperature module of FaIR is mathematically equivalent to the two-layer emulator in Equation (7.SM.2.1), and the emissions- or concentrations-to-ERF relationships in FaIR are equivalent or very similar to those described in generating the ERF time series in Section 7.SM.1. The similarity of the two-layer model to FaIR is demonstrated in Figure 7.SM.2.

The 1-million ensemble members sample the uncertainty in the ERF, the climate response and the carbon cycle. ERF uncertainties are generated using the same method described in Section 7.SM.1.3. For the climate response, the C , C_d , γ and ε components of the two-layer model in Equation 7.SM.2.1 are generated from kernel-density estimates that are calibrated to 44 CMIP6 models (Section 7.SM.2.1). The climate feedback parameter α is sampled from a truncated Gaussian distribution (truncated at ± 2 standard deviations) with mean $-1.33 \text{ W m}^{-2} ^{\circ}\text{C}^{-1}$ and standard deviation $0.5 \text{ W m}^{-2} ^{\circ}\text{C}^{-1}$. The carbon cycle in FaIR is parametrized by the pre-industrial time-integrated airborne fraction of CO₂, and the change in airborne fraction with accumulated carbon emissions and GSAT change (Millar et al., 2017). These parameters are sampled as uniform distributions using the lowest and highest values based on calibrations to 11 CMIP6 models (Arora et al., 2020) as the bounds of the distributions. The 1-million-member ensemble was run in the FaIR model using emissions-driven runs from 1750 to 2019. The resulting ensemble was constrained based on agreement to:

- i) The time series of historical GSAT to the Chapter 2 (Cross-Chapter Box 2.3) assessment from 1850–2020 with a root-mean-square error of 0.135°C or less, approximately recreating the headline 1850–1900 to 1995–2014 assessment of $0.67\text{--}0.98^{\circ}\text{C}$ (Cross Chapter Box 2.3, *very likely* range).
- ii) The assessment of ocean heat uptake from Section 7.2.2.2 from 1971–2018 within the *likely* range of 329–463 ZJ.
- iii) CO₂ concentrations to the 2014 *very likely* range of $397.1 \pm 0.4 \text{ ppm}$ (Table 2.1).
- iv) The airborne fraction from a 1% per year CO₂ increase simulation to the range assessed in Section 5.5.1 of $53 \pm 6\%$ (1 standard deviation).

From the original 1-million-member ensemble, 2237 ensemble members passed all four constraints and are used for reporting results. This constrained ensemble set from FaIRv1.6.2 has a good correspondence to assessed ranges of key climate metrics across the Working Group I report (Cross-Chapter Box 7.1, Tables 1 and 7.SM.4). While not used as formal constraints, the assessed distributions of ECS and TCR (Section 7.5.2) and projected future warming from the five

major SSP scenarios (Section 4.3.4) were used as guidelines to ensure simultaneous adherence to several assessed ranges. As a comparison, the ECS from this constrained set has a median and 5–95% ranges of ECS and TCR of 2.95 [2.05 to 5.07] °C and 1.81 [1.36 to 2.46] °C respectively, compared to the Chapter 7 best estimates and *very likely* ranges of 3.0 [2.0 to 5.0] °C for ECS and 1.8 [1.2 to 2.4] °C for TCR. While constraints (3) and (4) are not required when running FalR or the two-layer model using prescribed historical greenhouse gas concentrations, this 2237-member ensemble set is intended to be used to evaluate future warming pathways to integrated assessment model scenario projections in Chapter 3 of Working Group III, so the same ensemble set is used here for overall consistency.

7.SM.2.3 Supporting Information for Figures 7.7 and 7.8

The data contributing to Figures 7.7 and 7.8 is from the 2237-member constrained ensemble described in Section 7.SM.2.2. To provide the contributions to historical temperature in Figures 7.7 and 7.8, one of the 13 components of the historical forcing at a time is removed from the total forcing, and the two-layer model is run using the forcing and climate configuration from each of the 2237 ensemble members. The difference between the all-forcing and leave-one-out model run provides the temperature contribution from each forcing agent. This exercise was repeated using a best-estimate climate response (hence, only assessing the impact of uncertainty in the ERF) by setting ECS = 3.0°C, TCR 1.8°C and the other two-layer model parameters set to their CMIP6 model means ($C = 8.1 \text{ W yr m}^{-2} \text{ }^{\circ}\text{C}^{-1}$, $C_d = 110 \text{ W yr m}^{-2} \text{ }^{\circ}\text{C}^{-1}$, $\gamma = 0.64 \text{ W m}^{-2} \text{ }^{\circ}\text{C}^{-1}$ and $\varepsilon = 1.36$; Section 7.SM.2.1). These simulations are shown as dashed error bars in Figure 7.7, with the full ERF and climate response uncertainty as solid error bars.

Each ensemble member uses a long (approximately 9000-year) pre-industrial spin-up comprising only transient solar and volcanic forcing starting in 6755 BCE (Section 7.SM.1.3), and temperature changes are reported with respect to 1750 as a single baseline year. The same 2237-ensemble member set was extended forward in time to 2500 under forcing from the SSP scenarios (Section 7.SM.1.4) and used to inform global mean sea level projections in Chapter 9.

7.SM.2.4 Supporting information for Figure SPM.4b

A similar exercise was performed for the anthropogenic contributions to future warming shown in Figure SPM.4b. As no natural forcing is included in this exercise, a long pre-industrial spin-up is not required and only the period 1750–2100 was run using the constrained two-layer model. As in Section 7.SM.2.3, 2237 ensemble members are used, sampling the full assessed uncertainty ranges in effective radiative forcing and climate response. In these simulations, the baseline case is all anthropogenic forcing, with one component removed at a time and the differences in warming reported. Contributions to future warming are reported for CO₂, other non-CO₂ greenhouse gases (including ozone and stratospheric water vapor from methane oxidation), and other anthropogenic components. The latter category includes aerosols, land-use change, contrails and light-absorbing particles on snow and ice. The analysis is performed for SSP1-1.9, SSP1-2.6, SSP2-4.5, SSP3-7.0 and SSP5-8.5. Temperature projections are reported for 2081–2100 relative to a 1850–1900 baseline.

7.SM.3 Performance of Emulators Compared to Key Physical Climate Assessments

Table 7.SM.4 details the performance of the four emulators (CICERO-SCM, FalRv1.6.2, MAGICC7.5.1 and OSCARv3.1.1) described in Cross-Chapter Box 7.1 for a number of climate assessments in absolute terms, and can be compared to Cross-Chapter Box 7.1, Table 2 which details the relative difference between each emulator and the AR6-assessed range.

The comparison of the constrained two-layer emulator to FalRv1.6.2 and MAGICC7.5.1 is shown in Figure 7.SM.3 for the SSP1-2.6 and SSP5-8.5 scenarios, demonstrating the similarity between the FalR and two-layer projections as well as the similarity between FalR and MAGICC in their AR6 setups.

Table 7.SM.4 | Absolute differences between the emulator value and the Working Group I-assessed best estimate and range for key climate assessments. Values are given for four emulators in their respective AR6-calibrated probabilistic setups. Relative values of these indicators are shown in Cross-Chapter Box 7.1, Table 2. Emulator values within 5% of the assessed central value and 10% of the lower and upper ranges are unshaded, showing good correspondence between the emulator and the assessment. Progressively darker shading is applied to emulator values that are further from the assessed ranges. The columns labelled 'upper' and 'lower' indicate *very likely* (5–95%) ranges, except for the variables demarcated with an asterisk or double asterisk (* or **), where they denote *likely* ranges from 17–83%. Note that the TCRE-assessed range (**) is wider than the combination of the TCR and airborne fraction to account for uncertainties related to model limitations.

Emulator	Assessed Ranges			CICERO-SCM			FaIRv1.6.2			MAGICC7			OSCARv3.1.1			
Assessed Range	Lower	Central	Upper	Lower	Central	Upper	Lower	Central	Upper	Lower	Central	Upper	Lower	Central	Upper	
Key Metrics																
ECS (°C)	2.00	3.00	5.00	2.53	3.05	4.09	2.05	2.95	5.07	1.93	2.97	4.83	1.84	2.54	3.90	
TCRE (°C per 1000 GtC)**	1.00	1.65	2.30				1.29	1.53	1.82	1.37	1.73	2.19	1.50	1.52	1.83	
TCR (°C)	1.20	1.80	2.40	1.38	1.71	2.32	1.36	1.81	2.46	1.27	1.88	2.61	1.51	1.82	2.05	
Historical Warming and Effective Radiative Forcing																
GSAT Warming (°C)	1995–2014 relative to 1850–1900	0.67	0.85	0.98	0.68	0.85	0.98	0.72	0.87	1.02	0.72	0.86	0.97	0.67	0.78	0.98
Ocean Heat Content Change (ZJ)*	1971–2018	329	396	463	250	288	329	346	381	423	325	382	436	174	243	508
Total Aerosol ERF (W m ⁻²)	2005–2014 relative to 1750	-2.00	-1.30	-0.60	-1.27	-0.82	-0.54	-1.68	-1.15	-0.60	-1.79	-1.20	-0.55	-1.24	-1.11	-0.79
WMGHG ERF (W m ⁻²)	2019 relative to 1750	3.03	3.32	3.61	3.14	3.14	3.14	3.07	3.38	3.66	3.10	3.35	3.60	3.06	3.42	3.49
Methane ERF (W m ⁻²)	2019 relative to 1750	0.43	0.54	0.65	0.56	0.56	0.56	0.44	0.56	0.67	0.43	0.54	0.67	0.47	0.54	0.62
Carbon Cycle Metrics																
Airborne Fraction 1pctCO ₂ (dimensionless)*	2 × CO ₂	0.47	0.53	0.59				0.50	0.52	0.53	0.52	0.56	0.59	0.47	0.53	0.64
Airborne Fraction 1pctCO ₂ (dimensionless)*	4 × CO ₂	0.50	0.60	0.70				0.56	0.60	0.63	0.57	0.62	0.66	0.53	0.59	0.69
Future Warming (GSAT) Relative to 1995–2014																
SSP1-1.9 (°C)	2021–2040	0.38	0.61	0.85	0.42	0.58	0.94	0.39	0.61	0.94	0.39	0.61	0.88	0.43	0.55	0.64
	2041–2060	0.40	0.71	1.07	0.43	0.65	1.15	0.36	0.66	1.14	0.39	0.71	1.15	0.45	0.65	0.74
	2081–2100	0.24	0.56	0.96	0.21	0.42	0.94	0.18	0.48	1.00	0.20	0.52	0.99	0.26	0.51	0.66
SSP1-2.6 (°C)	2021–2040	0.41	0.63	0.89	0.44	0.60	0.94	0.42	0.64	0.96	0.40	0.62	0.89	0.45	0.57	0.64
	2041–2060	0.54	0.88	1.32	0.58	0.83	1.34	0.53	0.86	1.38	0.54	0.89	1.35	0.62	0.82	0.95
	2081–2100	0.51	0.90	1.48	0.50	0.78	1.41	0.47	0.84	1.49	0.48	0.89	1.49	0.59	0.82	1.05
SSP2-4.5 (°C)	2021–2040	0.44	0.66	0.90	0.48	0.63	0.94	0.47	0.65	0.92	0.45	0.64	0.89	0.42	0.57	0.63
	2041–2060	0.78	1.12	1.57	0.81	1.08	1.62	0.79	1.11	1.59	0.79	1.13	1.60	0.84	1.03	1.12
	2081–2100	1.24	1.81	2.59	1.22	1.63	2.51	1.21	1.75	2.63	1.21	1.82	2.67	1.34	1.74	1.96
SSP3-7.0 (°C)	2021–2040	0.45	0.67	0.92	0.50	0.64	0.93	0.51	0.68	0.91	0.49	0.68	0.92	0.43	0.57	0.65
	2041–2060	0.92	1.28	1.75	0.96	1.22	1.74	0.98	1.28	1.72	0.98	1.33	1.77	0.99	1.17	1.29
	2081–2100	2.00	2.76	3.75	1.99	2.55	3.64	2.07	2.72	3.72	2.13	2.86	3.97	2.09	2.59	2.81
SSP5-8.5 (°C)	2021–2040	0.51	0.76	1.04	0.54	0.71	1.06	0.56	0.77	1.08	0.55	0.77	1.06	0.51	0.66	0.73
	2041–2060	1.08	1.54	2.08	1.11	1.42	2.07	1.12	1.55	2.17	1.11	1.57	2.16	1.19	1.44	1.58
	2081–2100	2.44	3.50	4.82	2.54	3.24	4.68	2.58	3.50	4.89	2.63	3.65	5.16	2.65	3.35	3.62

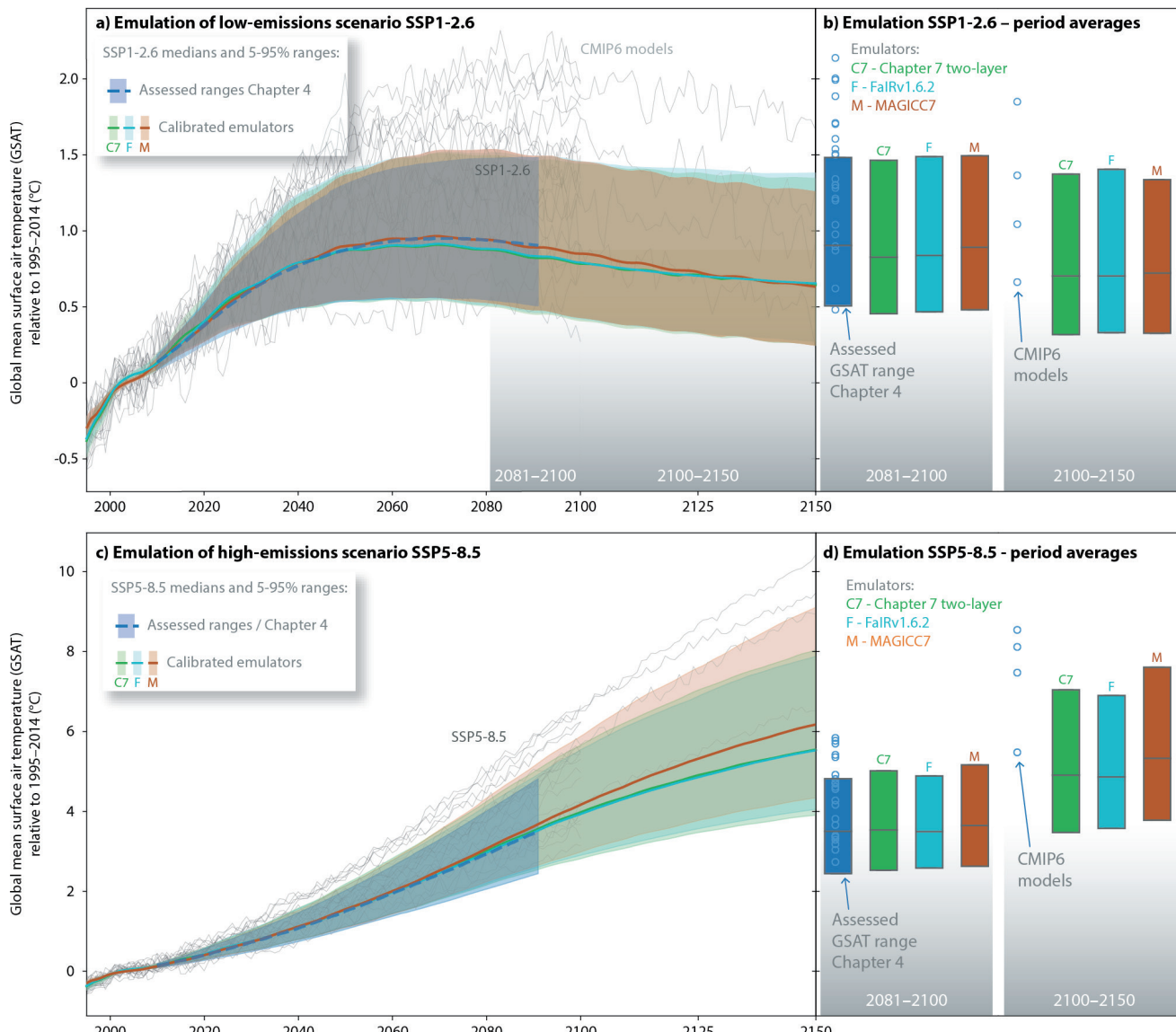


Figure 7.SM.2 | (a, c) Time series and (b, d) 2081–2100 and 2100–2150 means of emulated GSAT projections from the Chapter 7 two-layer model (green), FAIRv1.6.2 (light blue) and MAGICC7.5.1 (orange) from 1995 to 2150, following the SSP1-2.6 scenario (a and b) and the SSP5-8.5 scenario (c and d). In (a) and (c) the ensemble median estimates are solid lines and the 5–95% ranges are shaded; in (b) and (d) the bar range shows 5–95% ranges with the median in black. Overlaid CMIP6 model results are shown as lines in (a) and (c), and dots in (b) and (d); fewer dots are shown for the 2100–2150 period because only a limited number of CMIP6 models have performed runs beyond 2100. In (a) and (c), Chapter 4 assessed GSAT projections (20-year running means) are shown with a dark-blue dashed line and 5–95% range in dark-blue shading.

7.SM.4 Equilibrium Climate Sensitivity and Transient Climate Response from CMIP6 Models

Table 7.SM.5 details the equilibrium climate sensitivity and transient climate response estimated from CMIP6 and CMIP5 models using the ESMValTool (Eyring et al., 2020; Lauer et al., 2020; Righi et al., 2020) and presented in Schlund et al. (2020) for ECS and Meehl et al. (2020) for TCR (CMIP6 only), used in Section 7.5.6, Figure 7.18 and FAQ 7.3. Climate feedback parameters, including the decomposition into Planck, water vapour plus lapse rate, surface albedo and cloud components, plus the residual, are given for CMIP6 and CMIP5 models from Zelinka et al. (2020). ECS is estimated from a 150-year

integration of an *abrupt4xCO₂* experiment, subtracting the parallel piControl integration from the same period, regressing the modelled top-of-atmosphere energy imbalance ΔN against the modelled GSAT change ΔT , and taking $\Delta T/2$ at the point where the regression slope crosses $\Delta N = 0$ (Gregory et al., 2004). TCR is estimated from the mean ΔT change from a *1pctCO₂* run compared to the parallel piControl integration in years 60 to 79. Feedback contributions are estimated from a mean of six radiative kernels presented in Zelinka et al. (2020).

Table 7.SM.5 | Equilibrium climate sensitivity (ECS) and climate feedbacks estimated from CMIP5 and CMIP6 models. Transient climate response (TCR) from CMIP6 models is also provided. Data from Schlund et al. (2020), Meehl et al. (2020) and Zelinka et al. (2020).

MIP Era	Model	ECS °C	Net Feedback α , W m ⁻² °C ⁻¹	Components of the Net Feedback, W m ⁻² °C ⁻¹					TCR °C
				Planck	Water Vapour + Lapse Rate	Surface Albedo	Cloud	Residual	
CMIP6	ACCESS-CM2	4.72	-0.74	-3.22	1.18	0.37	0.80	0.14	2.10
	ACCESS-ESM1-5	3.87	-0.73	-3.21	1.33	0.42	0.62	0.11	1.95
	AWI-CM-1-1-MR	3.16	-1.15	-3.16	1.27	0.42	0.29	0.04	2.06
	BCC-CSM2-MR	3.04	-1.03	-3.25	1.23	0.38	0.57	0.04	1.72
	BCC-ESM1	3.26	-0.92	-3.23	1.24	0.42	0.58	0.06	1.77
	CAMS-CSM1-0	2.29	-1.82	-3.25	1.30	0.24	-0.30	0.20	1.73
	CAS-ESM2-0	3.51							2.04
	CESM2	5.16	-0.63	-3.28	1.26	0.38	1.01	-0.01	2.06
	CESM2-FV2	5.14	-0.55	-3.23	1.17	0.40	1.10	0.01	2.05
	CESM2-WACCM	4.75	-0.71	-3.27	1.25	0.37	1.22	-0.28	1.98
	CESM2-WACCM-FV2	4.79	-0.61	-3.24	1.16	0.37	1.17	-0.07	2.01
	CIESM		-0.69	-3.19	1.19	0.27	0.84	0.20	2.39
	CMCC-CM2-SR5	3.52	-1.07	-3.26	1.27	0.31	0.58	0.04	2.09
	CMCC-ESM2		-1.05	-3.25	1.29	0.33	0.56	0.02	
	CNRM-CM6-1	4.83	-0.74	-3.22	1.24	0.49	0.61	0.14	2.14
	CNRM-CM6-1-HR	4.28	-0.92	-3.27	1.27	0.37	0.59	0.13	2.48
	CNRM-ESM2-1	4.76	-0.62	-3.23	1.27	0.47	0.63	0.25	1.86
	CanESM5	5.62	-0.65	-3.26	1.29	0.42	0.88	0.03	2.74
	E3SM-1-0	5.32	-0.63	-3.27	1.25	0.32	0.97	0.11	2.99
	EC-Earth3		-0.76	-3.18	1.45	0.53	0.39	0.05	2.30
	EC-Earth3-AerChem		-0.94	-3.18	1.39	0.54	0.27	0.05	
	EC-Earth3-Veg	4.31	-0.78	-3.21	1.45	0.53	0.37	0.07	2.62
	FGOALS-f3-L	3.00	-1.40	-3.14	1.21	0.36	0.04	0.13	1.94
	FGOALS-g3	2.88	-1.25	-3.23	1.45	0.49	0.10	-0.06	1.54
	FIO-ESM-2-0								2.22
	GFDL-CM4		-0.82	-3.18	1.23	0.50	0.64	-0.01	
	GFDL-ESM4		-1.42	-3.25	1.18	0.34	0.50	-0.19	
	GISS-E2-1-G	2.72	-1.46	-3.20	1.06	0.24	0.07	0.38	1.80
	GISS-E2-1-H	3.11	-1.13	-3.16	1.27	0.42	0.06	0.28	1.93
	GISS-E2-2-G		-1.51	-3.19	1.18	0.32	0.01	0.18	1.71
	HadGEM3-GC31 LL	5.55	-0.63	-3.21	1.19	0.38	0.84	0.17	2.55
	HadGEM3-GC31-MM	5.42	-0.66	-3.23	1.18	0.32	0.91	0.16	2.58
	IITM-ESM		-1.91	-3.22	1.16	0.26	-0.02	-0.08	1.71
	INM-CM4-8	1.83	-1.48	-3.23	1.45	0.36	-0.09	0.02	1.33
	INM-CM5-0	1.92	-1.52	-3.23	1.40	0.40	-0.06	-0.03	
	IPSL-CM5A2-INCA		-0.81	-3.25	1.23	0.33	1.05	-0.16	
	IPSL-CM6A-LR	4.56	-0.76	-3.22	1.35	0.44	0.45	0.22	2.32
	KACE-1-0-G	4.75	-0.72	-3.24	1.17	0.33	0.84	0.18	2.04
	MCM-UA-1-0	3.65							1.94
	MIROC-ES2L	2.68	-1.54	-3.26	1.19	0.40	0.04	0.08	1.55
	MIROC6	2.61	-1.40	-3.29	1.30	0.47	0.22	-0.10	1.55
	MPI-ESM-1-2-HAM	2.96	-1.41	-3.10	1.18	0.36	-0.16	0.32	1.80

MIP Era	Model	ECS °C	Net Feedback $\alpha, \text{W m}^{-2} \text{ }^{\circ}\text{C}^{-1}$	Components of the Net Feedback, $\text{W m}^{-2} \text{ }^{\circ}\text{C}^{-1}$					TCR °C
				Planck	Water Vapour + Lapse Rate	Surface Albedo	Cloud	Residual	
CMIP6 (continued)	MPI-ESM1-2-HR	2.98	-1.22	-3.14	1.21	0.38	0.27	0.05	1.66
	MPI-ESM1-2-LR	3.00	-1.39	-3.11	1.12	0.37	0.18	0.05	1.84
	MRI-ESM2-0	3.15	-1.10	-3.20	1.16	0.54	0.46	-0.06	1.64
	NESM3	4.72	-0.78	-3.09	1.19	0.50	0.45	0.17	2.72
	NorCPM1	3.05	-1.10	-3.17	1.31	0.44	0.30	0.01	1.56
	NorESM2-LM	2.54	-1.34	-3.30	1.28	0.35	0.44	-0.11	1.48
	NorESM2-MM	2.50	-1.50	-3.32	1.29	0.30	0.51	-0.28	1.33
	SAM0-UNICON	3.72	-1.04	-3.27	1.13	0.38	0.75	-0.03	2.27
	TaiESM1	4.31	-0.88	-3.25	1.26	0.40	0.70	0.00	2.34
	UKESM1-0-LL	5.34	-0.67	-3.19	1.19	0.48	0.87	-0.01	2.79
CMIP6 Mean		3.78	-1.03	-3.22	1.25	0.39	0.49	0.05	2.01
CMIP6 Standard Deviation		1.08	0.36	0.05	0.09	0.08	0.38	0.14	0.41
CMIP5	ACCESS1-0	3.83	-0.76	-3.18	1.26	0.43	0.47	0.25	
	ACCESS1-3	3.53	-0.81	-3.21	1.25	0.41	0.65	0.08	
	BNU-ESM	3.92	-0.92	-3.14	1.35	0.61	0.20	0.05	
	CCSM4	2.94	-1.18	-3.19	1.28	0.48	0.27	-0.02	
	CNRM-CM5	3.25	-1.13	-3.20	1.24	0.46	0.15	0.21	
	CNRM-CM5-2	3.44							
	CSIRO-Mk3-6-0	4.08	-0.64	-3.26	1.25	0.38	0.67	0.32	
	CanESM2	3.69	-1.03	-3.28	1.35	0.39	0.52	-0.02	
	FGOALS-g2	3.38	-0.84	-3.18	1.40	0.59	0.38	-0.03	
	FGOALS-s2		-0.91	-3.19	1.32	0.52	0.03	0.42	
	GFDL-CM3	3.97	-0.76	-3.18	1.08	0.43	0.88	0.02	
	GFDL-ESM2G	2.39	-1.23	-3.20	1.17	0.30	0.22	0.27	
	GFDL-ESM2M	2.44	-1.37	-3.20	1.13	0.29	0.11	0.30	
	GISS-E2-H	2.31	-1.66	-3.16	1.27	0.32	-0.12	0.03	
	GISS-E2-R	2.11	-1.76	-3.17	1.30	0.24	-0.14	0.01	
	HadGEM2-ES	4.61	-0.63	-3.17	1.30	0.40	0.70	0.14	
	IPSL-CM5A-LR	4.13	-0.75	-3.26	1.20	0.27	1.18	-0.14	
	IPSL-CM5A-MR	4.12	-0.80	-3.28	1.18	0.19	1.25	-0.14	
	IPSL-CM5B-LR	2.60	-1.02	-3.17	1.32	0.28	0.62	-0.06	
	MIROC-ESM	4.67	-0.92	-3.32	1.23	0.50	0.68	-0.02	
	MIROC5	2.72	-1.53	-3.24	1.29	0.48	-0.04	-0.02	
	MPI-ESM-LR	3.63	-1.13	-3.16	1.09	0.44	0.44	0.06	
	MPI-ESM-MR	3.46	-1.19	-3.17	1.05	0.39	0.47	0.06	
	MPI-ESM-P	3.45	-1.23	-3.18	1.08	0.40	0.39	0.08	
	MRI-CGCM3	2.60	-1.23	-3.24	1.25	0.51	0.28	-0.03	
	NorESM1-M	2.80	-1.10	-3.17	1.32	0.45	0.29	0.01	
	NorESM1-ME		-1.10	-3.16	1.30	0.45	0.33	-0.01	
	bcc-csm1-1-m	2.86	-1.19	-3.27	1.29	0.40	0.40	0.00	
	bcc-csm1-1	2.83	-1.15	-3.21	1.27	0.45	0.28	0.05	
	inmcm4	2.08	-1.43	-3.18	1.23	0.43	0.24	-0.15	
CMIP5 mean		3.28	-1.08	-3.20	1.24	0.41	0.41	0.06	
CMIP5 standard deviation		0.74	0.29	0.05	0.09	0.10	0.33	0.14	

7.SM.5 Climate Metrics

7.SM.5.1 Definitions of Climate Metrics

Absolute Global Forcing Potential:

$$AGFP_X(H) = \Delta F_X(H) \quad (7.SM.5.1)$$

Absolute Global Warming Potential

$$AGWP_X(H) = \int_0^H \Delta F_X(t) dt \quad (7.SM.5.2)$$

Absolute Global Temperature-change Potential:

$$AGTP^X(H) = \Delta T^X(H) = \int_0^H AGFP^X(t) R_T(H-t) dt \quad (7.SM.5.3)$$

Absolute Global Sea Level Rise:

$$\begin{aligned} AGSR^X(H) &= \Delta SLR^X(H) = \int_0^H AGTP^X(t) R_{SLR}(H-t) dt \\ &= \int_0^H \int_0^t AGFP^X(t') R_T(t-t') R_{SLR}(H-t) dt' dt \end{aligned} \quad (7.SM.5.4)$$

where R_{SLR} is the sea level rise resulting from a pulse temperature increase (Sterner et al., 2014).

Increase in absolute metric ($\Delta AGxx^X$) due to the carbon cycle response:

$$\Delta AGxx^X = \int_0^H \int_0^t AGTP^X(t') \gamma r_F(t-t') AGxx^{CO2}(H-t) dt \quad (7.SM.5.5)$$

where $\gamma r_F(t)$ is the CO_2 flux perturbation following a unit temperature pulse in $kg CO_2 yr^{-1} K^{-1}$ using the parametrization of Gasser et al. (2017b):

$$r_F = \delta(t) - \frac{\alpha_1}{\tau_1} e^{-\frac{t}{\tau_1}} - \frac{\alpha_2}{\tau_2} e^{-\frac{t}{\tau_2}} - \frac{\alpha_3}{\tau_3} e^{-\frac{t}{\tau_3}} \quad (7.SM.5.6)$$

The parameters used in Equations (7.SM.5.5) and (7.SM.5.6) are given in Table 7.SM.6.

Metrics for step-emission changes can be derived by integrating the more standard pulse-emission changes up to the time horizon:

$$AGTP_X^S = \int_0^H AGTP_X(H-t) dt \quad (7.SM.5.7)$$

The contribution to methane-emission metrics from CO_2 from fossil methane oxidation is given by

$$\Delta AGxx^X = \int_0^H Y \frac{m_{CO_2}}{m_{CH_4}} \frac{1}{\tau_{OH}} e^{-\frac{(H-t)}{\tau_{OH}}} AGxx^{CO2}(t) dt \quad (7.SM.5.8)$$

where Y is the fractional molar yield of CO_2 from CH_4 oxidation (see Section 7.6.1.3), m_{CO_2} and m_{CH_4} are the molar masses of CO_2 and CH_4 , and τ_{OH} is the methane-oxidation lifetime to OH (9.7 yr; Section 6.3.1).

7.SM.5.2 Impulse-Response Functions for GTP and Chapter 6 Calculations

To generate a suite of two-layer configurations for uncertainty estimates in GTP calculations (Tables 7.SM.8–7.SM.13), information from the FalRv1.6.2 and MAGICC7.5.1 AR6 calibration setups (Cross-Chapter Box 7.1) are used. FalRv1.6.2 uses the two-layer model in Equation (7.SM.2.1) as its core so converting its parameters to two-layer configurations is trivial (discussed in Section 7.SM.2.2). To convert MAGICC7.5.1's configuration to two-layer configurations, the two-layer model parameters are fitted to MAGICC7.5.1's output from an abrupt $2 \times CO_2$ experiment. However, such a fitting procedure produces only an approximate translation because MAGICC7.5.1 is not well represented by a two-time-scale model. After these two conversions are done an ensemble of two-layer configurations is generated which is used for uncertainty analysis in GTP calculations.

To generate the Chapter 6 two-layer configuration, the time scales and efficacy parameters are calculated as the average of FalRv1.6.2's median and a fit to MAGICC7.5.1's median response (both in their AR6 calibrations). Response magnitudes that describe the contributions to the fast and slow response time scales are calculated such that the Chapter 6 configuration matches the best-estimate ECS of $3.0^\circ C$ and TCR of $1.8^\circ C$ (Table 7.13) under the best-estimate ERF due to a doubling of CO_2 of $3.93 W m^{-2}$. This results in parameter values for $C = 7.7 W yr^{-2} ^\circ C^{-1}$, $C_d = 147 W yr^{-2} ^\circ C^{-1}$, $\alpha = -1.31 W m^{-2} ^\circ C^{-1}$, $\varepsilon = 1.03$, $\kappa = 0.88 W m^{-2} ^\circ C^{-1}$. Note these parameters differ from CMIP6 two-layer model calibrations in Section 7.SM.2.1, as the set described here is derived from a constrained ensemble from two emulators.

Table 7.SM.6 | Parameters for the carbon cycle response function (from Table 1 of Gasser et al., 2017b).

γ ($kg CO_2 yr^{-1} ^\circ C^{-1}$)	α_1	α_2	α_3	τ_1 (yr)	τ_2 (yr)	τ_3 (yr)
11.06×10^{12}	0.6368	0.3322	0.0310	2.376	30.14	490.1

7.SM.6 Tables of Greenhouse Gas Lifetimes, Radiative Efficiencies and Metrics

Table 7.SM.7 | Greenhouse gas lifetimes, radiative efficiencies, global warming potentials (GWP_s), global temperature potentials (GTP_s) and cumulative global temperature potentials (CGTP_s). GWP_s given for 20-year, 100-year and 500-year time horizons. GTP_s and CGTP_s given for 50-year and 100-year time horizons. Note CGTP has units of years and is applied to a change in emissions rate rather than a change in emissions amount. Also shown are absolute values of GWP_s and GTP_s (AGWP_s and AGTP_s), in units of picowatt years per square metre per kilogram ($1 \text{ pW} = 10^{-12} \text{ W}$) or picokelvin per kilogram ($1 \text{ pK} = 10^{-12} \text{ K}$). Radiative efficiencies for CH₄ and N₂O given in this table do not include chemical adjustments (values including chemical adjustments are given in Table 7.15). For SF₆ the assessed lifetime from Section 2.2.4.3 is used, all other lifetimes are taken from Hodnebrog et al. (2020).

Name	Formula	Lifetime (yr)	Radiative Efficiency (W m ⁻² ppb ⁻¹)	AGWP-20 (pW m ⁻² yr kg ⁻¹)	GWP-20	AGWP-100 (pW m ⁻² yr kg ⁻¹)	GWP-100	AGWP-500 (pW m ⁻² yr kg ⁻¹)	GWP-500	AGTP-50 (pK kg ⁻¹)	GTP-50	AGTP-100 (pK kg ⁻¹)	GTP-100	CGTP-50 (yr)	CGTP-100 (yr)
Major Greenhouse Gases															
Carbon dioxide	CO ₂		1.33×10^{-5}	0.0243	1	0.0895	1	0.314	1	0.000428	1	0.000395	1		
Methane ¹	CH ₄	11.8	0.000388	1.98	81.2	2.49	27.9	2.5	7.95	0.00473	11	0.00212	5.38	2730	3320
Nitrous oxide	N ₂ O	109	0.0032	6.65	273	24.5	273	40.7	130	0.124	290	0.0919	233		
Chlorofluorocarbons															
CFC-11	CCl ₃ F	52	0.291	203	8320	557	6230	657	2090	2.72	6350	1.40	3540		
CFC-12	CCl ₂ F ₂	102	0.358	310	12700	1120	12500	1790	5700	5.67	13300	4.10	10400		
CFC-13	CClF ₃	640	0.278	301	12400	1450	16200	5500	17500	7.26	17000	7.4	18800		
CFC-112	CCl ₂ FCCl ₂ F	63.6	0.282	137	5620	413	4620	525	1670	2.06	4810	1.19	3020		
CFC-112a	CCl ₃ CClF ₂	52	0.246	115	4740	317	3550	374	1190	1.55	3620	0.795	2010		
CFC-113	CCl ₂ FCClF ₂	93	0.301	167	6860	583	6520	890	2830	2.96	6910	2.06	5210		
CFC-113a	CCl ₃ CF ₃	55	0.241	124	5110	351	3930	422	1350	1.73	4030	0.917	2320		
CFC-114	CClF ₂ CClF ₂	189	0.314	201	8260	844	9430	1930	6150	4.28	9990	3.71	9410		
CFC-114a	CCl ₂ FCF ₃	105	0.297	183	7510	664	7420	1080	3450	3.37	7880	2.46	6240		
CFC-115	CClF ₂ CF ₃	540	0.246	180	7410	859	9600	3100	9880	4.3	10100	4.33	11000		
E-R316c	trans cyc (-CClFCF ₂ CF ₂ CClF-)	75	0.27	117	4810	379	4230	518	1650	1.91	4450	1.2	3040		
Z-R316c	cis cyc (-CClFCF ₂ CF ₂ CClF-)	114	0.3	136	5590	507	5660	865	2760	2.57	6020	1.94	4910		
CFC 1112	CClF=CClF	0.019	0.013	0.0111	0.454	0.0113	0.126	0.0113	0.036	1.18×10^{-5}	0.028	8.96×10^{-6}	0.023	12.9	15.3
CFC 1112a	CCl ₂ =CF ₂	0.006	0.007	0.00184	0.076	0.00188	0.021	0.00188	0.006	1.97×10^{-6}	0.005	1.49×10^{-6}	0.004	2.16	2.55
Hydrofluorochlorocarbons															
HCFC-21	CHCl ₂ F	1.7	0.145	14	575	14.3	160	14.3	45.6	0.0152	35.5	0.0114	29	16300	19400
HCFC-22	CHClF ₂	11.9	0.214	139	5690	175	1960	176	560	0.336	785	0.15	379	192000	234000
HCFC-31	CH ₂ ClF	1.2	0.068	6.96	286	7.11	79.4	7.11	22.6	0.00752	17.6	0.00567	14.4	8130	9630

¹ The methane metrics in this supplementary table are presented without accounting for the carbon content of the methane to enable users to undertake separate carbon budgeting. Examples of budgeting for “fossil” and “non-fossil” methane are provided in the Chapter 7 Table 7.15.

Name	Formula	Lifetime (yr)	Radiative Efficiency (W m ⁻² ppb ⁻¹)	AGWP-20 (pW m ⁻² yr kg ⁻¹)	GWP-20	AGWP-100 (pW m ⁻² yr kg ⁻¹)	GWP-100	AGWP-500 (pW m ⁻² yr kg ⁻¹)	GWP-500	AGTP-50 (pK kg ⁻¹)	GTP-50	AGTP-100 (pK kg ⁻¹)	GTP-100	CGTP-50 (yr)	CGTP-100 (yr)
Major Greenhouse Gases															
HCFC-121	CHCl ₂ CCl ₂ F	1.11	0.146	5.11	210	5.22	58.3	5.22	16.6	0.00552	12.9	0.00416	10.5	5970	7070
HCFC-122	CHCl ₂ CClF ₂	0.9	0.159	4.94	203	5.05	56.4	5.05	16.1	0.00533	12.5	0.00403	10.2	5780	6850
HCFC-122a	CHClFCCl ₂ F	3.1	0.201	21.4	879	21.9	245	21.9	69.9	0.0236	55.3	0.0177	44.7	25000	29600
HCFC-123	CHCl ₂ CF ₃	1.3	0.16	7.92	325	8.09	90.4	8.09	25.8	0.00857	20	0.00646	16.4	9260	11000
HCFC-123a	CHClFCClF ₂	4	0.227	34.3	1410	35.3	395	35.3	113	0.0385	90	0.0285	72.3	40200	47700
HCFC-124	CHClFCF ₃	5.9	0.207	50.3	2070	53.4	597	53.4	170	0.0612	143	0.0435	110	60500	71900
HCFC-124a	CHF ₂ CCl ₂ F	17	0.25	124	5110	185	2070	186	592	0.521	1220	0.177	448	192000	244000
HCFC-132	CHClFCHClF	1.73	0.143	10.7	440	11	122	11	34.9	0.0116	27.2	0.00876	22.2	12500	14800
HCFC-132a	CHCl ₂ CHF ₂	1.12	0.127	6.17	253	6.3	70.4	6.3	20.1	0.00666	15.6	0.00503	12.7	7210	8540
HCFC-132c	CH ₂ FCCl ₂ F	4.1	0.169	29.6	1220	30.6	342	30.6	97.6	0.0334	78.1	0.0247	62.7	34800	41300
HCFC-133a	CH ₂ CICF ₃	4.6	0.15	33.4	1370	34.7	388	34.7	111	0.0382	89.3	0.0281	71.3	39400	46800
HCFC-141	CH ₂ CICHClF	1.14	0.072	4.08	168	4.17	46.6	4.17	13.3	0.00441	10.3	0.00333	8.43	4770	5650
HCFC-141b	CH ₃ CCl ₂ F	9.4	0.161	65.9	2710	77	860	77	246	0.115	269	0.064	162	85800	103000
HCFC-142b	CH ₃ CClF ₂	18	0.193	134	5510	205	2300	207	658	0.611	1430	0.203	514	211000	271000
HCFC-225ca	CHCl ₂ CF ₂ CF ₃	1.9	0.219	12	491	12.2	137	12.2	39	0.013	30.4	0.00979	24.8	14000	16600
HCFC-225cb	CHClFCF ₂ CClF ₂	5.9	0.293	47.8	1960	50.8	568	50.8	162	0.0582	136	0.0414	105	57500	68300
HCFO-1233zd(E)	(E)-CF ₃ CH=CHCl	0.116	0.065	0.34	14	0.347	3.88	0.347	1.11	0.000364	0.851	0.000276	0.7	398	471
HCFO-1233zd(Z)	(Z)-CF ₃ CH=CHCl	0.036	0.025	0.0398	1.64	0.0406	0.454	0.0406	0.129	4.25×10^{-5}	0.099	3.23×10^{-5}	0.082	46.6	55.2
(e)-1-chloro-2-fluoroethene	(E/Z)-CHCl=CHF	0.005	0.001	0.00032	0.013	0.000327	0.004	0.000327	0.001	3.42×10^{-7}	0.001	2.6×10^{-6}	0.001	0.375	0.444
Hydrofluorocarbons															
HFC-23	CHF ₃	228	0.191	301	12400	1310	14600	3300	10500	6.6	15400	5.95	15100		
HFC-32	CH ₂ F ₂	5.4	0.111	65.5	2690	69	771	69	220	0.0775	181	0.0561	142	78200	92900
HFC-41	CH ₃ F	2.8	0.025	11.8	485	12.1	135	12.1	38.6	0.013	30.4	0.00972	24.6	13800	16400
HFC-125	CHF ₂ CF ₃	30	0.234	164	6740	335	3740	349	1110	1.41	3300	0.512	1300		
HFC-134	CHF ₂ CHF ₂	10	0.194	95	3900	113	1260	113	361	0.18	420	0.0944	239	126000	151500
HFC-134a	CH ₂ FCF ₃	14	0.167	101	4140	137	1530	137	436	0.314	733	0.121	306	147000	181000
HFC-143	CH ₂ FCHF ₂	3.6	0.128	31.7	1300	32.6	364	32.6	104	0.0353	82.6	0.0263	66.6	37100	44000
HFC-143a	CH ₃ CF ₃	51	0.168	191	7840	520	5810	609	1940	2.53	5910	1.28	3250		
HFC-152	CH ₂ FCH ₂ F	0.471	0.045	1.89	77.6	1.93	21.5	1.93	6.14	0.00203	4.74	0.00153	3.89	2210	2610
HFC-152a	CH ₃ CHF ₂	1.6	0.102	14.4	591	14.7	164	14.7	46.8	0.0156	36.5	0.0118	29.8	16800	19900

Name	Formula	Lifetime (yr)	Radiative Efficiency (W m ⁻² ppb ⁻¹)	AGWP-20 (pW m ⁻² yr kg ⁻¹)	GWP-20	AGWP-100 (pW m ⁻² yr kg ⁻¹)	GWP-100	AGWP-500 (pW m ⁻² yr kg ⁻¹)	GWP-500	AGTP-50 (pK kg ⁻¹)	GTP-50	AGTP-100 (pK kg ⁻¹)	GTP-100	CGTP-50 (yr)	CGTP-100 (yr)
Major Greenhouse Gases															
HFC-161	CH ₃ CH ₂ F	0.219	0.016	0.424	17.4	0.433	4.84	0.433	1.38	0.000454	1.06	0.000344	0.872	497	588
HFC-227ca	CF ₃ CF ₂ CHF ₂	30	0.264	131	5370	267	2980	278	885	1.12	2620	0.407	1030		
HFC-227ea	CF ₃ CHFCF ₃	36	0.273	142	5850	322	3600	345	1100	1.45	3400	0.588	1490		
HFC-236cb	CH ₂ FCF ₂ CF ₃	13.4	0.231	91.2	3750	121	1350	121	387	0.265	620	0.106	268	131000	161000
HFC-236ea	CHF ₂ CHFCF ₃	11.4	0.3	108	4420	134	1500	134	428	0.245	572	0.114	288	147000	179000
HFC-236fa	CF ₃ CH ₂ CF ₃	213	0.251	181	7450	777	8690	1900	6040	3.93	9200	3.5	8870		
HFC-245ca	CH ₂ FCF ₂ CHF ₂	6.6	0.24	65.3	2680	70.5	787	70.5	225	0.0836	196	0.0576	146	79600	94700
HFC-245cb	CF ₃ CF ₂ CH ₃	39.9	0.251	170	6970	407	4550	445	1420	1.89	4410	0.817	2070		
HFC-245ea	CHF ₂ CHFCF ₂	3.2	0.16	22.2	912	22.8	255	22.8	72.6	0.0246	57.4	0.0183	46.5	26000	30800
HFC-245eb	CH ₂ FCF ₂ CF ₃	3.2	0.204	28.3	1160	29	325	29.1	92.6	0.0313	73.2	0.0234	59.2	33100	39200
HFC-245fa	CHF ₂ CH ₂ CF ₃	7.9	0.245	77.1	3170	86.1	962	86.1	274	0.112	262	0.0708	180	96700	115000
HFC-263fb	CH ₃ CH ₂ CF ₃	1.1	0.1	6.55	269	6.69	74.8	6.69	21.3	0.00707	16.5	0.00534	13.5	7660	9070
HFC-272ca	CH ₃ CF ₂ CH ₃	9	0.08	46.4	1910	53.6	599	53.6	171	0.0771	180	0.0444	113	59900	71800
HFC-329p	CHF ₂ CF ₂ CF ₂ CF ₃	32	0.313	122	5010	259	2890	272	866	1.12	2610	0.421	1070		
HFC-365mfc	CH ₃ CF ₂ CH ₂ CF ₃	8.9	0.228	71.1	2920	81.7	914	81.8	261	0.117	272	0.0677	172	91400	109000
HFC-43-10mee	CF ₃ CHFCF ₂ CF ₃	17	0.357	96.3	3960	143	1600	144	458	0.403	943	0.137	347	149000	189000
HFO-1123	CHF=CF ₂	0.004	0.002	0.000414	0.017	0.000423	0.005	0.000423	0.001	4.42×10^{-7}	0.001	3.36×10^{-7}	0.001	0.485	0.574
HFO-1132a	CH ₂ =CF ₂	0.013	0.004	0.0046	0.189	0.00469	0.052	0.00469	0.015	4.91×10^{-6}	0.011	3.73×10^{-6}	0.009	5.39	6.37
HFO-1141	CH ₂ =CHF	0.007	0.002	0.00213	0.088	0.00217	0.024	0.00218	0.007	2.28×10^{-6}	0.005	1.73×10^{-6}	0.004	2.5	2.95
HFO-1225ye(Z)	(Z)-CF ₃ CF=CHF	0.027	0.025	0.0302	1.24	0.0308	0.344	0.0308	0.098	3.23×10^{-5}	0.075	2.45×10^{-5}	0.062	35.3	41.8
HFO-1225ye(E)	(E)-CF ₃ CF=CHF	0.016	0.015	0.0104	0.426	0.0106	0.118	0.0106	0.034	1.11×10^{-5}	0.026	8.41×10^{-6}	0.021	12.1	14.4
HFO-1234ze(Z)	(Z)-CF ₃ CH=CHF	0.027	0.02	0.0276	1.13	0.0282	0.315	0.0282	0.09	2.95×10^{-5}	0.069	2.24×10^{-5}	0.057	32.3	38.2
HFO-1234ze(E)	(E)-CF ₃ CH=CHF	0.052	0.045	0.12	4.94	0.123	1.37	0.123	0.391	0.000129	0.3	9.75×10^{-5}	0.247	141	167
HFO-1234yf	CF ₃ CF=CH ₂	0.033	0.026	0.044	1.81	0.0449	0.501	0.0449	0.143	4.7×10^{-5}	0.11	3.57×10^{-5}	0.09	51.5	60.9
HFO-1336mzz(E)	(E)-CF ₃ CH=CHCF ₃	0.334	0.132	1.57	64.3	1.6	17.9	1.6	5.09	0.00168	3.92	0.00127	3.22	1830	2170
HFO-1336mzz(Z)	(Z)-CF ₃ CH=CHCF ₃	0.074	0.069	0.182	7.48	0.186	2.08	0.186	0.592	0.000195	0.455	0.000148	0.374	213	252
HFO-1243zf	CF ₃ CH=CH ₂	0.025	0.015	0.0229	0.94	0.0234	0.261	0.0234	0.074	2.45×10^{-5}	0.057	1.86×10^{-5}	0.047	26.8	31.7
HFO-1345zfc	CF ₃ CF ₂ CH=CH ₂	0.025	0.016	0.016	0.656	0.0163	0.182	0.0163	0.052	1.71×10^{-5}	0.04	1.29×10^{-5}	0.033	18.7	22.1
3,3,4,4,5,5,6,6, 6-nonafluorohex- 1-ene	n-C ₄ F ₉ CH=CH ₂	0.025	0.03	0.0179	0.734	0.0182	0.204	0.0182	0.058	1.91×10^{-5}	0.045	1.45×10^{-5}	0.037	20.9	24.7

Name	Formula	Lifetime (yr)	Radiative Efficiency (W m ⁻² ppb ⁻¹)	AGWP-20 (pW m ⁻² yr kg ⁻¹)	GWP-20	AGWP-100 (pW m ⁻² yr kg ⁻¹)	GWP-100	AGWP-500 (pW m ⁻² yr kg ⁻¹)	GWP-500	AGTP-50 (pK kg ⁻¹)	GTP-50	AGTP-100 (pK kg ⁻¹)	GTP-100	CGTP-50 (yr)	CGTP-100 (yr)
Major Greenhouse Gases															
3,3,4,4,5,5,6,6,7,7,8,8,8-trideca-fluorooct-1-ene	n-C ₆ F ₁₃ CH=CH ₂	0.025	0.034	0.0142	0.584	0.0145	0.162	0.0145	0.046	1.52 × 10 ⁻⁵	0.036	1.15 × 10 ⁻⁵	0.029	16.6	19.7
3,3,4,4,5,5,6,6,7,7,8,8,9,9,10,10,10-heptadeca-fluorodec-1-ene	n-C ₈ F ₁₇ CH=CH ₂	0.025	0.038	0.0124	0.508	0.0126	0.141	0.0126	0.04	1.32 × 10 ⁻⁵	0.031	0.00001	0.025	14.5	17.1
3,3,3-trifluoro-2-(trifluoromethyl)prop-1-ene	(CF ₃) ₂ C=CH ₂	0.028	0.033	0.0331	1.36	0.0337	0.377	0.0337	0.107	3.53 × 10 ⁻⁵	0.083	2.68 × 10 ⁻⁵	0.068	38.7	45.8
1,1,2,2,3,3-hexa-fluorocyclopentane	cyc (-CF ₂ CF ₂ CF ₂ CH ₂ CH ₂ -)	1.6	0.2	10.5	431	10.7	120	10.7	34.2	0.0114	26.6	0.00857	21.7	12300	14500
1,1,2,2,3,3,4-heptafluorocyclopentane	cyc (-CF ₂ CF ₂ CF ₂ CHFCH ₂ -)	2.8	0.243	20.2	830	20.7	231	20.7	66	0.0222	52	0.0166	42.1	23600	28000
1,3,3,4,4,5,5-heptafluorocyclopentene	cyc (-CF ₂ CF ₂ CF ₂ CF=CH-)	0.61	0.215	3.95	162	4.03	45.1	4.03	12.8	0.00424	9.92	0.00321	8.14	4620	5470
(4s,5s)-1,1,2,2,3,3,4,5-octafluorocyclopentane	trans-cyc (-CF ₂ CF ₂ CF ₂ CHFCHF-)	3.2	0.259	22.5	925	23.1	258	23.1	73.6	0.0249	58.2	0.0186	47.1	26300	31200
HFO-1438ezy(E)	(E)-(CF ₃) ₂ CFCH=CHF	0.334	0.079	0.721	29.6	0.736	8.22	0.736	2.34	0.000773	1.81	0.000585	1.48	843	998
HFO-1447fz	CF ₃ (CF ₂) ₂ CH=CH ₂	0.025	0.028	0.0206	0.847	0.021	0.235	0.021	0.067	2.2 × 10 ⁻⁵	0.051	1.67 × 10 ⁻⁵	0.042	24.1	28.6
1,3,3,4,4-penta-fluorocyclo-butene	cyc (-CH=CFCF ₂ CF ₂ -)	0.74	0.27	8.1	333	8.27	92.4	8.27	26.4	0.00872	20.4	0.00659	16.7	9470	11200
3,3,4,4-tetra-fluorocyclo-butene	cyc (-CH=CHCF ₂ CF ₂ -)	0.23	0.21	2.24	92.1	2.29	25.6	2.29	7.29	0.0024	5.61	0.00182	4.61	2620	3100
Chlorocarbons and Hydrochlorocarbons															
Methyl chloroform	CH ₃ CCl ₃	5	0.065	13.8	567	14.4	161	14.4	46	0.016	37.5	0.0117	29.7	16400	19400
Carbon tetrachloride	CCl ₄	32	0.166	92.7	3810	196	2200	206	658	0.849	1990	0.32	810		
Methyl chloride	CH ₃ Cl	0.9	0.005	0.485	19.9	0.495	5.54	0.496	1.58	0.000523	1.22	0.000395	1	567	672
Methylene chloride	CH ₂ Cl ₂	0.493	0.029	0.978	40.2	0.998	11.2	0.998	3.18	0.00105	2.46	0.000795	2.01	1140	1350
Chloroform	CHCl ₃	0.501	0.074	1.81	74.2	1.84	20.6	1.84	5.87	0.00194	4.53	0.00147	3.72	2110	2500

Name	Formula	Lifetime (yr)	Radiative Efficiency (W m ⁻² ppb ⁻¹)	AGWP-20 (pW m ⁻² yr kg ⁻¹)	GWP-20	AGWP-100 (pW m ⁻² yr kg ⁻¹)	GWP-100	AGWP-500 (pW m ⁻² yr kg ⁻¹)	GWP-500	AGTP-50 (pK kg ⁻¹)	GTP-50	AGTP-100 (pK kg ⁻¹)	GTP-100	CGTP-50 (yr)	CGTP-100 (yr)
Major Greenhouse Gases															
Nitrogen trifluoride	NF ₃	569	0.204	326	13400	1560	17400	5720	18200	7.81	18200	7.89	20000		
Pentadecafluoro-triethylamine	N(C ₂ F ₅) ₃	1000	0.61	188	7700	923	10300	3860	12300	4.61	10800	4.81	12200		
Perfluorotripropylamine	N(CF ₂ CF ₂ CF ₃) ₃	1000	0.75	164	6750	808	9030	3380	10800	4.03	9430	4.21	10700		
Heptacosafaurotributylamine	N(CF ₂ CF ₂ CF ₂ CF ₃) ₃	1000	0.907	154	6340	759	8490	3170	10100	3.79	8860	3.96	10000		
Perfluorotri-pentylamine	N(CF ₂ CF ₂ CF ₂ CF ₂ CF ₃) ₃	1000	0.95	132	5420	650	7260	2720	8650	3.24	7580	3.39	8580		
Heptafluoroisobutyronitrile	(CF ₃) ₂ CFCN	34.5	0.248	111	4580	246	2750	262	835	1.09	2560	0.431	1090		
Sulphur hexafluoride	SF ₆	1000	0.567	442	18200	2180	24300	9100	29000	10.9	25400	11.4	28800		
Trifluoromethyl-sulfur pentafluoride	SF ₅ CF ₃	800	0.585	339	13900	1660	18500	6610	21100	8.27	19300	8.54	21600		
Sulfuryl fluoride	SO ₂ F ₂	36	0.211	183	7510	414	4630	444	1410	1.87	4360	0.756	1920		
PFC-14	CF ₄	50000	0.099	129	5300	660	7380	3320	10600	3.28	7660	3.57	9050		
PFC-116	C ₂ F ₆	10000	0.261	218	8940	1110	12400	5500	17500	5.51	12900	5.99	15200		
PFC-218	C ₃ F ₈	2600	0.27	165	6770	831	9290	3890	12400	4.13	9660	4.44	11200		
Hexafluorocyclobutene	cyc (-CF=CFCF ₂ CF ₂ -)	1.02	0.3	11	453	11.3	126	11.3	35.9	0.0119	27.8	0.00898	22.8	12900	15300
PFC-C-318	cyc (-CF ₂ CF ₂ CF ₂ CF ₂ -)	3200	0.314	180	7400	912	10200	4330	13800	4.53	10600	4.88	12400		
PFC-31-10	n-C ₄ F ₁₀	2600	0.369	178	7300	897	10000	4200	13400	4.46	10400	4.79	12100		
Octafluorocyclopentene	cyc (-CF=CFCF ₂ CF ₂ CF ₂ -)	1.1	0.246	6.84	281	6.99	78.1	6.99	22.3	0.00739	17.3	0.00557	14.1	8000	9470
PFC-41-12	n-C ₅ F ₁₂	4100	0.408	163	6680	825	9220	3970	12700	4.1	9580	4.43	11200		
PFC-51-14	n-C ₆ F ₁₄	3100	0.449	153	6260	771	8620	3660	11600	3.83	8960	4.12	10500		
PFC-61-16	n-C ₇ F ₁₆	3000	0.503	149	6120	752	8410	3560	11300	3.74	8740	4.02	10200		
PFC-71-18	n-C ₈ F ₁₈	3000	0.558	146	6010	739	8260	3500	11100	3.67	8590	3.95	10000		
PFC-91-18	C ₁₀ F ₁₈	2000	0.537	133	5480	669	7480	3070	9780	3.33	7790	3.56	9010		

Name	Formula	Lifetime (yr)	Radiative Efficiency (W m^{-2} ppb^{-1})	AGWP-20 (pW m^{-2} yr kg^{-1})	GWP-20	AGWP-100 (pW m^{-2} yr kg^{-1})	GWP-100	AGWP-500 (pW m^{-2} yr kg^{-1})	GWP-500	AGTP-50 (pK kg^{-1})	GTP-50	AGTP-100 (pK kg^{-1})	GTP-100	CGTP-50 (yr)	CGTP-100 (yr)	
Major Greenhouse Gases																
1,1,2,2,3,3,4,4, 4a,5,5,6,6,7,7, 8,8,8a-octade- ca-fluoronaph- thalene	Z-C ₁₀ F ₁₈	2000	0.56	139	5710	698	7800	3200	10200	3.47	8120	3.71	9400			
1,1,2,2,3,3,4,4, 4a,5,5,6,6,7,7,8, 8,8a-octade- ca-fluoronaphtha- lene	E-C ₁₀ F ₁₈	2000	0.512	127	5220	637	7120	2920	9310	3.17	7420	3.39	8580			
PFC-1114	CF ₂ =CF ₂	0.003	0.002	0.000347	0.014	0.000354	0.004	0.000354	0.001	3.71×10^{-7}	0.001	2.81×10^{-7}	0.001	0.406	0.481	
PFC-1216	CF ₃ CF=CF ₂	0.015	0.013	0.00788	0.324	0.00804	0.09	0.00804	0.026	8.42×10^{-6}	0.02	6.39×10^{-6}	0.016	9.23	10.9	
1,1,2,3,4,4-hex- fluorobuta-1,3- diene	CF ₂ =CFCF=CF ₂	0.003	0.003	0.000347	0.014	0.000354	0.004	0.000354	0.001	3.71×10^{-7}	0.001	2.82×10^{-7}	0.001	0.407	0.481	
Octafluoro-1- butene	CF ₃ CF ₂ CF=CF ₂	0.016	0.019	0.00891	0.366	0.00909	0.102	0.00909	0.029	9.52×10^{-6}	0.022	7.22×10^{-5}	0.018	10.4	12.3	
Octafluoro-2- buene	CF ₃ CF=CFCF ₃	0.085	0.07	0.173	7.1	0.176	1.97	0.176	0.562	0.000185	0.432	0.00014	0.355	202	239	
Halogenated Alcohols, Ethers, Furans, Aldehydes and Ketones																
HFE-125	CHF ₂ OCF ₃	135	0.417	328	13500	1280	14300	2410	7680	6.5	15200	5.17	13100			
HFE-134	CHF ₂ OCHF ₂	26.9	0.449	310	12700	593	6630	610	1940	2.37	5530	0.814	2060			
HFE-143a	CH ₃ OCF ₃	4.9	0.189	52.8	2170	55.1	616	55.1	176	0.0611	143	0.0447	113	62600	74300	
HFE-227ea	CF ₃ CHFOCF ₃	54.8	0.459	238	9800	673	7520	808	2570	3.3	7720	1.75	4440			
HCFE-235ca2	CHF ₂ OCF ₂ CHFCl	4.42	0.409	56.4	2320	58.5	654	58.5	186	0.0642	150	0.0473	120	66500	78900	
HCFE-235da2	CHF ₂ OCHClCF ₃	3.5	0.426	46.9	1930	48.2	539	48.2	154	0.0522	122	0.0388	98.4	54900	65100	
HFE-236ea2	CHF ₂ OCHFCF ₃	14.1	0.464	171	7020	232	2590	233	741	0.537	1260	0.206	521	249000	308000	
HFE-236fa	CF ₃ CH ₂ OCF ₃	7.5	0.371	89.4	3670	98.7	1100	98.8	315	0.125	291	0.0811	205	111000	133000	
HFE-245cb2	CF ₃ CF ₂ OCH ₃	5	0.336	64	2630	66.9	747	66.9	213	0.0743	174	0.0542	137	75900	90100	
HFE-245fa1	CHF ₂ CH ₂ OCF ₃	6.7	0.314	77.2	3170	83.6	934	83.6	266	0.0998	233	0.0683	173	94300	112000	
HFE-245fa2	CHF ₂ OCH ₂ CF ₃	5.5	0.36	74.5	3060	78.6	878	78.6	251	0.0886	207	0.0639	162	89000	106000	
2,2,3,3,3-penta- fluoropropan-1-ol	CF ₃ CF ₂ CH ₂ OH	0.471	0.164	3.01	123	3.07	34.3	3.07	9.78	0.00323	7.54	0.00244	6.19	3520	4160	
HFE-254cb1	CH ₃ OCF ₂ CHF ₂	2.5	0.26	28.7	1180	29.3	328	29.3	93.5	0.0314	73.4	0.0235	59.6	33500	39700	
HFE-263mf	CF ₃ CH ₂ OCH ₃	0.077	0.046	0.181	7.43	0.184	2.06	0.185	0.588	0.000193	0.452	0.000147	0.371	212	250	

Name	Formula	Lifetime (yr)	Radiative Efficiency (W m ⁻² ppb ⁻¹)	AGWP-20 (pW m ⁻² yr kg ⁻¹)	GWP-20	AGWP-100 (pW m ⁻² yr kg ⁻¹)	GWP-100	AGWP-500 (pW m ⁻² yr kg ⁻¹)	GWP-500	AGTP-50 (pK kg ⁻¹)	GTP-50	AGTP-100 (pK kg ⁻¹)	GTP-100	CGTP-50 (yr)	CGTP-100 (yr)
Major Greenhouse Gases															
HFE-263m1	CF ₃ OCH ₂ CH ₃	0.397	0.126	2.56	105	2.61	29.2	2.61	8.32	0.00274	6.42	0.00208	5.27	2990	3540
3,3,3-trifluoro-propan-1-ol	CF ₃ CH ₂ CH ₂ OH	0.041	0.026	0.0544	2.23	0.0555	0.62	0.0555	0.177	5.81 × 10 ⁻⁵	0.136	4.41 × 10 ⁻⁵	0.112	63.7	75.3
HFE-329mcc2	CHF ₂ CF ₂ OCF ₂ CF ₃	25	0.545	184	7550	337	3770	345	1100	1.29	3020	0.432	1090		
HFE-338mmz1	(CF ₃) ₂ CHOCHF ₂	22.3	0.452	158	6500	272	3040	276	880	0.967	2260	0.314	797		
HFE-338mcf2	CF ₃ CH ₂ OCF ₂ CF ₃	7.5	0.454	84.2	3460	93	1040	93.1	297	0.117	274	0.0764	194	105000	125000
HFE-347mmz1	(CF ₃) ₂ CHOCH ₂ F	1.9	0.308	17.1	702	17.5	195	17.5	55.7	0.0186	43.5	0.014	35.4	20000	23600
HFE-347mcc3	CH ₃ OCF ₂ CF ₂ CF ₃	5.1	0.339	49.2	2020	51.5	576	51.6	164	0.0574	134	0.0418	106	58500	69400
HFE-347mcf2	CHF ₂ CH ₂ OCF ₂ CF ₃	6.7	0.431	79.6	3270	86.2	963	86.2	275	0.103	241	0.0705	179	97300	116000
HFE-347pcf2	CHF ₂ CF ₂ OCH ₂ CF ₃	6.1	0.482	82.1	3370	87.6	980	87.7	279	0.101	237	0.0715	181	99100	118000
HFE-347mmmy1	(CF ₃) ₂ CFOCH ₃	3.7	0.318	34.1	1400	35.1	392	35.1	112	0.0381	89	0.0283	71.8	40000	47400
HFE-356mec3	CH ₃ OCF ₂ CHFCF ₃	2.5	0.288	23.1	949	23.6	264	23.6	75.3	0.0253	59.2	0.019	48	27000	32000
HFE-356mff2	CF ₃ CH ₂ OCH ₂ CF ₃	0.351	0.19	2.14	88	2.19	24.4	2.19	6.97	0.0023	5.37	0.00174	4.41	2510	2970
HFE-356pcf2	CHF ₂ CH ₂ OCF ₂ CHF ₂	6	0.378	69.8	2870	74.4	831	74.4	237	0.0856	200	0.0606	154	84100	100000
HFE-356pcf3	CHF ₂ OCH ₂ CF ₂ CHF ₂	3.5	0.378	42.1	1730	43.3	484	43.3	138	0.0469	110	0.0349	88.4	49300	58500
HFE-356pcc3	CH ₃ OCF ₂ CF ₂ CHF ₂	2.5	0.303	24.2	995	24.8	277	24.8	79	0.0266	62.1	0.0199	50.4	28300	33500
HFE-356mmz1	(CF ₃) ₂ CHOCH ₃	0.178	0.125	0.713	29.3	0.728	8.13	0.728	2.32	0.000763	1.78	0.000579	1.47	835	988
HFE-365mcf3	CF ₃ CF ₂ CH ₂ OCH ₃	0.069	0.058	0.141	5.77	0.143	1.6	0.143	0.457	0.00015	0.351	0.000114	0.289	164	195
HFE-374pcf2	CHF ₂ CF ₂ OCH ₂ CH ₃	0.208	0.132	1.1	45	1.12	12.5	1.12	3.56	0.00117	2.74	0.000889	2.25	1280	1520
4,4,4-trifluoro-butan-1-ol	CF ₃ (CH ₂) ₂ CH ₂ OH	0.015	0.006	0.00433	0.178	0.00442	0.049	0.00442	0.014	4.63 × 10 ⁻⁵	0.011	3.51 × 10 ⁻⁵	0.009	5.08	6.01
2,2,3,3,4,4,5,5-octafluorocyclopentan-1-ol	cyc -(CF ₃) ₄ CH(OH)-	0.301	0.156	1.2	49.1	1.22	13.6	1.22	3.89	0.00128	3	0.000971	2.46	1400	1660
HFE-43-10pccc124	CHF ₂ OCF ₂ OCF ₂ CF ₂ OCHF ₂	14.1	1.03	212	8720	288	3220	289	920	0.667	1560	0.255	647	309000	383000
HFE-449s1	C ₄ F ₉ OCH ₃	4.8	0.36	39.5	1620	41.2	460	41.2	131	0.0455	106	0.0334	84.6	46700	55500
n-HFE-7100	CF ₃ CF ₂ CF ₂ CF ₂ OCH ₃	4.8	0.425	46.7	1920	48.6	544	48.7	155	0.0538	126	0.0394	99.9	55200	65600
i-HFE-7100	(CF ₃) ₂ CFCF ₂ OCH ₃	4.8	0.341	37.5	1540	39.1	437	39.1	124	0.0432	101	0.0317	80.2	44300	52600
HFE-569sf2	C ₄ F ₉ OC ₂ H ₅	0.8	0.301	5.32	219	5.43	60.7	5.43	17.3	0.00573	13.4	0.00433	11	6220	7370
i-HFE-7200	(CF ₃) ₂ CFCF ₂ OCH ₃	0.63	0.216	3.01	124	3.07	34.3	3.07	9.78	0.00323	7.56	0.00245	6.2	3520	4160

Name	Formula	Lifetime (yr)	Radiative Efficiency (W m^{-2} ppb^{-1})	AGWP-20 (pW m^{-2} yr kg^{-1})	GWP-20	AGWP-100 (pW m^{-2} yr kg^{-1})	GWP-100	AGWP-500 (pW m^{-2} yr kg^{-1})	GWP-500	AGTP-50 (pK kg^{-1})	GTP-50	AGTP-100 (pK kg^{-1})	GTP-100	CGTP-50 (yr)	CGTP-100 (yr)	
Major Greenhouse Gases																
HFE-7300	(CF ₃) ₂ CFCFOC ₂ H ₅ CF ₂ CF ₃	5.24	0.48	34.5	1420	36.2	405	36.2	115	0.0405	94.7	0.0294	74.6	41100	48800	
HFE-7500	n-C ₃ F ₇ CFOC ₂ H ₅ CF(CF ₃) ₂	0.3	0.27	1.14	47	1.17	13	1.17	3.72	0.00123	2.86	0.000928	2.35	1340	1580	
HFE-236ca12	CHF ₂ OCF ₂ OCHF ₂	26.5	0.648	285	11700	542	6060	557	1770	2.15	5020	0.733	1860			
HFE-338pcc13	CHF ₂ OCF ₂ CF ₂ OCHF ₂	13.4	0.87	223	9180	297	3320	297	948	0.649	1520	0.259	657	321000	395000	
1,1,1,3,3,3-hexa-fluoropropan-2-ol	(CF ₃) ₂ CHOH	1.9	0.274	18.1	742	18.5	206	18.5	58.8	0.0197	46	0.0148	37.4	21100	25000	
HG-02	CHF ₂ (OCF ₂ CF ₂) ₂ OCHF ₂	26.9	1.15	268	11000	513	5730	528	1680	2.05	4780	0.704	1780			
HG-03	CHF ₂ (OCF ₂ CF ₂) ₃ OCHF ₂	26.9	1.43	250	10300	479	5350	492	1570	1.91	4470	0.657	1660			
Fluroxene	CF ₃ CH ₂ OCH=CH ₂	0.01	0.011	0.00505	0.207	0.00515	0.058	0.00515	0.016	5.39×10^{-5}	0.013	4.09×10^{-6}	0.01	5.91	6.99	
2-ethoxy-3,3,4,4,5-pentafluorotetrahydro-2,5-bis[1,2,2,2-tetrafluoro-1-(trifluoromethyl)ethyl]-furan	C ₁₂ H ₅ F ₁₉ O ₂	0.81	0.489	4.27	175	4.36	48.7	4.36	13.9	0.0046	10.7	0.00347	8.8	4990	5910	
Difluoro(methoxy)methane	CH ₃ OCHF ₂	1.1	0.153	11.9	491	12.2	136	12.2	38.9	0.0129	30.1	0.00973	24.7	14000	16500	
HG'-01	CH ₃ OCF ₂ CF ₂ OCH ₃	1.7	0.289	17.7	727	18.1	202	18.1	57.7	0.0192	45	0.0145	36.7	20700	24500	
HG'-02	CH ₃ O(CF ₂ CF ₂ O) ₂ CH ₃	1.7	0.562	20	823	20.5	229	20.5	65.3	0.0218	50.9	0.0164	41.5	23400	27700	
HG'-03	CH ₃ O(CF ₂ CF ₂ O) ₃ CH ₃	1.7	0.762	19.2	789	19.6	219	19.6	62.5	0.0209	48.8	0.0157	39.8	22400	26600	
HFE-329me3	CF ₃ CFHCF ₂ OCF ₃	33.6	0.489	180	7410	393	4390	416	1330	1.73	4040	0.671	1700			
3,3,4,4,5,5,6,6,7,7,7-undeca-fluoroheptan-1-ol	CF ₃ (CF ₂) ₄ CH ₂ CH ₂ OH	0.047	0.054	0.0468	1.92	0.0477	0.533	0.0477	0.152	5×10^{-5}	0.117	3.79×10^{-5}	0.096	54.8	64.8	
3,3,4,4,5,5,6,6,7,7,8,8,9,9,9-pentadecafluoronon-1-ol	CF ₃ (CF ₂) ₆ CH ₂ CH ₂ OH	0.047	0.06	0.0394	1.62	0.0401	0.449	0.0402	0.128	4.21×10^{-5}	0.098	3.19×10^{-5}	0.081	46.1	54.5	

Name	Formula	Lifetime (yr)	Radiative Efficiency (W m^{-2} ppb^{-1})	AGWP-20 (pW m^{-2} yr kg^{-1})	GWP-20	AGWP-100 (pW m^{-2} yr kg^{-1})	GWP-100	AGWP-500 (pW m^{-2} yr kg^{-1})	GWP-500	AGTP-50 (pK kg^{-1})	GTP-50	AGTP-100 (pK kg^{-1})	GTP-100	CGTP-50 (yr)	CGTP-100 (yr)	
Major Greenhouse Gases																
3,3,4,4,5,5,6,6,7, 7,8,8,9,9,10,10, 11,11,11-nona-decafluoroundecan-1-ol	$\text{CF}_3(\text{CF}_2)_8\text{CH}_2\text{CH}_2\text{OH}$	0.047	0.045	0.024	0.985	0.0245	0.273	0.0245	0.078	2.56×10^{-5}	0.06	1.94×10^{-5}	0.049	28.1	33.2	
2-chloro-1,1, 2-trifluoro-1-methoxyethane	$\text{CH}_3\text{OCF}_2\text{CHClF}$	1.43	0.211	11.9	488	12.1	136	12.1	38.7	0.0129	30.1	0.0097	24.6	13900	16400	
PFPMIE	$\text{CF}_3\text{OCFCF}_3\text{CF}_2\text{O}$ CF_2OCF_3	800	0.64	189	7750	920	10300	3680	11700	4.59	10700	4.75	12000			
HFE-216	$\text{CF}_3\text{OCF}=\text{CF}_2$	0.004	0.006	0.000909	0.037	0.000927	0.01	0.000928	0.003	9.71×10^{-7}	0.002	7.37×10^{-7}	0.002	1.06	1.26	
Perfluoroethyl formate	$\text{CF}_3\text{CF}_2\text{OCHO}$	3.6	0.408	51.9	2130	53.4	597	53.4	170	0.0579	135	0.0431	109	60800	72100	
2,2,2-trifluoroethyl formate	$\text{CF}_3\text{CH}_2\text{OCHO}$	0.548	0.192	4.8	197	4.9	54.8	4.9	15.6	0.00516	12.1	0.0039	9.89	5620	6650	
Formic acid;1,1,1, 3,3,3-hexafluoropropan-2-ol	$(\text{CF}_3)_2\text{CHOCHO}$	3.1	0.255	23.5	964	24.1	269	24.1	76.7	0.0259	60.6	0.0194	49	27400	32500	
Ethenyl 2,2,2-trifluoroacetate	$\text{CF}_3\text{COOCH}=\text{CH}_2$	0.004	0.004	0.000705	0.029	0.000719	0.008	0.000719	0.002	7.52×10^{-7}	0.002	5.71×10^{-7}	0.001	0.825	0.976	
Ethyl 2,2,2-trifluoroacetate	$\text{CF}_3\text{COOCH}_2\text{CH}_3$	0.06	0.056	0.139	5.7	0.142	1.58	0.142	0.451	0.000148	0.347	0.000112	0.285	162	192	
Prop-2-enyl 2,2,2-trifluoroacetate	$\text{CF}_3\text{COOCH}_2\text{CH}=\text{CH}_2$	0.003	0.005	0.000636	0.026	0.000648	0.007	0.000649	0.002	6.79×10^{-7}	0.002	5.15×10^{-7}	0.001	0.745	0.881	
Methyl 2,2,2-trifluoroacetate	$\text{CF}_3\text{COOCH}_3$	1	0.158	7.21	296	7.36	82.3	7.36	23.5	0.00778	18.2	0.00587	14.9	8430	9980	
2,2,3,3,4,4,4-heptafluorobutan-1-ol	$\text{CF}_3\text{CF}_2\text{CF}_2\text{CH}_2\text{OH}$	0.55	0.199	3.2	131	3.26	36.5	3.26	10.4	0.00343	8.03	0.0026	6.58	3740	4430	
1,1,2-trifluoro-2-(trifluoromethoxy)ethane	$\text{CHF}_2\text{CHFOCF}_3$	9	0.353	97.6	4010	113	1260	113	359	0.162	379	0.0933	236	126000	151000	
1-ethoxy-1,1,2,3,3,3-hexafluoropropane	$\text{CF}_3\text{CHFCF}_2\text{OCH}_2\text{CH}_3$	0.403	0.193	2.32	95.2	2.37	26.4	2.37	7.54	0.00249	5.81	0.00188	4.77	2710	3210	

Name	Formula	Lifetime (yr)	Radiative Efficiency (W m^{-2} ppb^{-1})	AGWP-20 (pW m^{-2} yr kg^{-1})	GWP-20	AGWP-100 (pW m^{-2} yr kg^{-1})	GWP-100	AGWP-500 (pW m^{-2} yr kg^{-1})	GWP-500	AGTP-50 (pK kg^{-1})	GTP-50	AGTP-100 (pK kg^{-1})	GTP-100	CGTP-50 (yr)	CGTP-100 (yr)	
Major Greenhouse Gases																
1,1,1,2,2,3, 3-heptafluoro-3- (1,2,2,2-tetra- fluoroethoxy) propane	<chem>CF3CF2CF2OCHFCF3</chem>	59.4	0.591	202	8320	593	6630	733	2340	2.94	6860	1.63	4140			
2,2,3,3-tetra- fluoropropan-1-ol	<chem>CHF2CF2CH2OH</chem>	0.255	0.112	1.27	52	1.29	14.4	1.29	4.12	0.00136	3.17	0.00103	2.6	1480	1750	
2,2,3,4,4,4- hexafluoro- butan-1-ol	<chem>CF3CHFCF2CH2OH</chem>	0.367	0.227	2.67	110	2.73	30.5	2.73	8.69	0.00287	6.7	0.00217	5.5	3130	3700	
1,1,2,2-tetra- fluoro-3-meth- oxypropane	<chem>CHF2CF2CH2OCH3</chem>	0.071	0.052	0.147	6.03	0.15	1.68	0.15	0.478	0.000157	0.367	0.000119	0.302	172	203	
1,1,1,2,2,4,5,5, 5-nonafluoro-4- (trifluoromethyl) pentan-3-one	<chem>CF3CF2COCF(CF3)2</chem>	0.019	0.028	0.01	0.411	0.0102	0.114	0.0102	0.033	1.07×10^{-5}	0.025	8.12×10^{-5}	0.021	11.7	13.9	
3,3,3-trifluoro- propanal	<chem>CF3CH2CHO</chem>	0.008	0.005	0.00221	0.091	0.00225	0.025	0.00225	0.007	2.36×10^{-5}	0.006	1.79×10^{-5}	0.005	2.58	3.06	
2-fluoroethanol	<chem>CH2FCH2OH</chem>	0.044	0.012	0.0465	1.91	0.0474	0.53	0.0474	0.151	4.97×10^{-5}	0.116	3.77×10^{-5}	0.095	54.4	64.4	
2,2-difluoro- ethanol	<chem>CHF2CH2OH</chem>	0.167	0.046	0.542	22.3	0.553	6.18	0.553	1.76	0.00058	1.36	0.00044	1.11	634	751	
2,2,2-trifluoro- ethanol	<chem>CF3CH2OH</chem>	0.458	0.117	3.13	129	3.2	35.7	3.2	10.2	0.00336	7.86	0.00254	6.44	3660	4340	
HG-04	<chem>CHF2O(CF2CF2O)4CHF2</chem>	26.9	1.46	204	8400	392	4380	403	1280	1.56	3660	0.538	1360			
Methyl-perfluoro- heptene-ethers	<chem>CH3OCF13</chem>	0.304	0.27	1.32	54.4	1.35	15.1	1.35	4.3	0.00142	3.31	0.00107	2.72	1550	1830	
1,1,1-trifluoro- propan-2-one	<chem>CF3COCH3</chem>	0.014	0.011	0.00788	0.324	0.00804	0.09	0.00804	0.026	8.42×10^{-5}	0.02	6.39×10^{-5}	0.016	9.23	10.9	
1,1,1-trifluoro- butan-2-one	<chem>CF3COCH2CH3</chem>	0.018	0.01	0.00834	0.343	0.00851	0.095	0.00851	0.027	8.91×10^{-5}	0.021	6.76×10^{-5}	0.017	9.77	11.6	
1-chloro-2-ethen- oxyethane	<chem>ClCH2CH2OCH=CH2</chem>	0	0.001	1.65×10^{-5}	0.001	1.68×10^{-5}	0	1.68×10^{-5}	0	1.76×10^{-8}	0	1.33×10^{-8}	0	0.019	0.023	
2-methylpentan- 3-one	<chem>CH3CH2COCH(CH3)2</chem>	0.015	0.02	0.0175	0.719	0.0179	0.2	0.0179	0.057	1.87×10^{-5}	0.044	1.42×10^{-5}	0.036	44.8	53	
Ethyl methyl ether	<chem>CH3CH2OCH3</chem>	0.005	0.002	0.000856	0.035	0.000873	0.01	0.000873	0.003	9.14×10^{-7}	0.002	6.94×10^{-7}	0.002	2.04	2.42	

Name	Formula	Lifetime (yr)	Radiative Efficiency (W m ⁻² ppb ⁻¹)	AGWP-20 (pW m ⁻² yr kg ⁻¹)	GWP-20	AGWP-100 (pW m ⁻² yr kg ⁻¹)	GWP-100	AGWP-500 (pW m ⁻² yr kg ⁻¹)	GWP-500	AGTP-50 (pK kg ⁻¹)	GTP-50	AGTP-100 (pK kg ⁻¹)	GTP-100	CGTP-50 (yr)	CGTP-100 (yr)
Major Greenhouse Gases															
Octafluoro-oxolane	C ₄ F ₈ O	3000	0.463	246	10100	1240	13900	5890	18800	6.18	14500	6.65	16900		
Crotonaldehyde	CH ₃ CH=CHCHO	0.001	0	0	0	0	0	0	0	0	0	0	0	0	0
Methyl vinyl ketone	CH ₃ COCH=CH ₂	0.001	0	2.48 × 10 ⁻⁵	0.001	2.53 × 10 ⁻⁵	0	2.53 × 10 ⁻⁵	0	2.64 × 10 ⁻⁸	0	2.01 × 10 ⁻⁸	0	0.029	0.034
Allyl ether	(CH ₂ =CHCH ₂) ₂ O	0	0.001	1.19 × 10 ⁻⁵	0	1.22 × 10 ⁻⁵	0	1.22 × 10 ⁻⁵	0	1.27 × 10 ⁻⁸	0	9.65 × 10 ⁻⁹	0	0.014	0.017
Allyl ethyl ether	CH ₃ CH ₂ OCH ₂ CH=CH ₂	0.001	0.001	3.39 × 10 ⁻⁵	0.001	3.46 × 10 ⁻⁵	0	3.46 × 10 ⁻⁵	0	3.62 × 10 ⁻⁸	0	2.75 × 10 ⁻⁸	0	0.04	0.047
(z)-hex-2-en-1-ol	CH ₃ CH ₂ CH ₂ CH=CHCH ₂ OH	0	0.038	0.000223	0.009	0.000228	0.003	0.000228	0.001	2.38 × 10 ⁻⁷	0.001	1.81 × 10 ⁻⁷	0	0.261	0.309
(e)-hex-2-en-1-ol	CH ₃ CH ₂ CH ₂ CH=CHCH ₂ OH	0	0.036	0.000208	0.009	0.000212	0.002	0.000212	0.001	2.22 × 10 ⁻⁷	0.001	1.68 × 10 ⁻⁷	0	0.243	0.288
Miscellaneous Compounds															
Allyl cyanide	CH ₂ =CHCH ₂ CN	0.002	0	4.08 × 10 ⁻⁵	0.002	4.16 × 10 ⁻⁵	0	4.16 × 10 ⁻⁵	0	4.35 × 10 ⁻⁸	0	3.3 × 10 ⁻⁸	0	0.048	0.056
Hexamethyl-disiloxane	C ₆ H ₁₈ OSi ₂	0.025	0.047	0.0418	1.72	0.0426	0.476	0.0426	0.136	4.46 × 10 ⁻⁵	0.104	3.39 × 10 ⁻⁵	0.086	48.9	57.9
Octamethyltrisiloxane	C ₈ H ₂₄ O ₂ Si ₃	0.019	0.06	0.0285	1.17	0.029	0.325	0.029	0.093	3.04 × 10 ⁻⁵	0.071	2.31 × 10 ⁻⁵	0.058	33.3	39.4
Decamethyl-tetrasiloxane	C ₁₀ H ₃₀ O ₃ Si ₄	0.014	0.06	0.0155	0.635	0.0158	0.176	0.0158	0.05	1.65 × 10 ⁻⁵	0.039	1.25 × 10 ⁻⁵	0.032	18.1	21.4
Dodecamethyl-pentasiloxane	C ₁₂ H ₃₆ O ₄ Si ₅	0.011	0.064	0.0107	0.439	0.0109	0.122	0.0109	0.035	1.14 × 10 ⁻⁵	0.027	8.67 × 10 ⁻⁶	0.022	12.5	14.8
Hexamethyl-cyclotrisiloxane	C ₆ H ₁₈ O ₃ Si ₃	0.038	0.1	0.101	4.14	0.103	1.15	0.103	0.328	0.000108	0.252	8.18 × 10 ⁻⁵	0.207	118	140
Octamethylcyclo-tetrasiloxane	C ₈ H ₂₄ O ₄ Si ₄	0.027	0.12	0.0648	2.66	0.0661	0.739	0.0661	0.211	6.92 × 10 ⁻⁵	0.162	5.25 × 10 ⁻⁵	0.133	75.9	89.8
Decamethylcyclo-pentasiloxane	C ₁₀ H ₃₀ O ₅ Si ₅	0.016	0.098	0.0253	1.04	0.0258	0.289	0.0259	0.082	2.71 × 10 ⁻⁵	0.063	2.05 × 10 ⁻⁵	0.052	29.7	35.1
Dodecamethyl-cyclohexasiloxane	C ₁₂ H ₃₆ O ₆ Si ₆	0.011	0.086	0.0124	0.51	0.0127	0.142	0.0127	0.04	1.33 × 10 ⁻⁵	0.031	1.01 × 10 ⁻⁵	0.026	14.6	17.2
Ethane	C ₂ H ₆	0.159	0.001	0.0383	1.57	0.0391	0.437	0.0391	0.125	4.1 × 10 ⁻⁵	0.096	3.11 × 10 ⁻⁵	0.079	0.048	0.056
Propane	C ₃ H ₈	0.036	0	0.00175	0.072	0.00178	0.02	0.00178	0.006	1.87 × 10 ⁻⁶	0.004	1.42 × 10 ⁻⁶	0.004	48.9	57.9
Butane	n-C ₄ H ₁₀	0.019	0	0.000542	0.022	0.000553	0.006	0.000553	0.002	5.79 × 10 ⁻⁷	0.001	4.4 × 10 ⁻⁷	0.001	33.3	39.4

Table 7.SM.8 | Estimated uncertainty in the global warming potential (GWP) and global temperature-change potential (GTP) for CH₄ showing the total uncertainty as a percentage of the best estimate (expressed as 5–95% confidence interval), and the uncertainty by component of the total emission metric calculation (radiative efficiency, chemistry feedbacks, atmospheric lifetime, CO₂ (combined uncertainty in radiative efficiency and CO₂ impulse response)), carbon cycle response, fate of oxidized fossil methane, and impulse-response function. Uncertainties in individual terms are taken from Section 7.6, except for the CO₂ impulse response which comes from Joos et al. (2013). The impulse-response uncertainties are calculated by taking 1.645 × standard deviation of the GTPs generated from 600 ensemble members of the impulse response derived from FalRv1.6.2 and MAGICC7.5.1 (Section 7.SM.4.2).

Metric	Percentage Uncertainty in the Metric Best Estimate Due to:							Total Uncertainty (%)
	Radiative Efficiency (%)	Chemical Response (%)	Lifetime (%)	CO ₂ (%)	Carbon Cycle (%)	Fossil Fuel Oxidation (%)	Impulse-response Function (%)	
GWP-20	20	14	9	18	3	2	0	32
GWP-100	20	14	14	26	5	7	0	40
GWP-500	20	14	14	29	5	26	0	48
GTP-50	20	14	37	22	17	22	31	64
GTP-100	20	14	18	28	8	60	38	83

Table 7.SM.9 | As Table 7.SM.8, for N₂O.

Metric	Percentage Uncertainty in the Metric Best Estimate Due to:						Total Uncertainty (%)
	Radiative Efficiency (%)	Chemical Response (%)	Lifetime (%)	CO ₂ (%)	Carbon Cycle (%)	Impulse-response Function (%)	
GWP-20	16	36	1	18	2	0	43
GWP-100	16	36	3	26	5	0	47
GWP-500	16	36	8	29	5	0	49
GTP-50	16	36	3	25	6	1	46
GTP-100	16	36	7	29	6	2	49

Table 7.SM.10 | As Table 7.SM.8, for CFC-11.

Metric	Percentage Uncertainty in the Metric Best Estimate Due to:					Total Uncertainty (%)
	Radiative Efficiency (%)	Lifetime (%)	CO ₂ (%)	Carbon Cycle (%)	Impulse-response Function (%)	
GWP-20	22	3	18	2	0	29
GWP-100	22	12	26	5	0	37
GWP-500	22	19	29	5	0	42
GTP-50	22	14	24	6	4	37
GTP-100	22	28	28	7	7	47

Table 7.SM.11 | As Table 7.SM.8, for PFC-14 (CF₄).

Metric	Percentage Uncertainty in the Metric Best Estimate Due to:					Total Uncertainty (%)
	Radiative Efficiency (%)	Lifetime (%)	CO ₂ (%)	Carbon Cycle (%)	Impulse-response Function (%)	
GWP-20	19	0	18	2	0	26
GWP-100	19	0	26	4	0	33
GWP-500	19	0	29	5	0	35
GTP-50	19	0	25	5	2	32
GTP-100	19	0	29	5	1	35

Table 7.SM.12 | As Table 7.SM.8, for HFC-134a.

Metric	Percentage Uncertainty in the Metric Best Estimate Due to:					Total Uncertainty (%)
	Radiative Efficiency (%)	Lifetime (%)	CO ₂ (%)	Carbon Cycle (%)	Impulse-response Function (%)	
GWP-20	19	10	18	3	0	28
GWP-100	19	19	26	5	0	38
GWP-500	19	19	29	5	0	40
GTP-50	19	47	22	14	25	62
GTP-100	19	30	28	9	37	59

Table 7.SM.13 | As Table 7.SM.8, for HFC-32.

Metric	Percentage Uncertainty in the Metric Best Estimate Due to:					Total Uncertainty (%)
	Radiative Efficiency (%)	Lifetime (%)	CO ₂ (%)	Carbon Cycle (%)	Impulse-response Function (%)	
GWP-20	19	17	18	3	0	31
GWP-100	19	19	26	5	0	38
GWP-500	19	19	29	5	0	40
GTP-50	19	22	19	26	48	65
GTP-100	19	19	29	7	39	56

7.SM.7 Data Table

Table 7.SM.14 | Input data table. Input datasets and code used to create chapter figures.

Figure Number	Dataset/Code Name	Type	File Name/Specificities	License Type	Dataset/Code Citation	Dataset/Code URL	Related Publications
Box 7.2, Figure 1		Code	notebooks/350_chapter7_box7.2_fig1.ipynb	MIT		https://github.com/IPCC-WG1/Chapter-7 (accessed 28/01/2022)	
		Data	data_input/fig7.1_box7.2/			https://github.com/IPCC-WG1/Chapter-7 (accessed 28/01/2022)	
Figure 7.3		Code	notebooks/300_chapter7_fig7.3.ipynb	MIT		https://github.com/IPCC-WG1/Chapter-7 (accessed 28/01/2022)	
		Data	data_input/Loeb_et_al_2020			https://github.com/IPCC-WG1/Chapter-7 (accessed 28/01/2022)	Loeb et al. (2020)
Figure 7.4		Code	notebooks/270_chapter7_fig7.4.ipynb	MIT	Smith et al. (2021)	https://github.com/IPCC-WG1/Chapter-7 (accessed 28/01/2022)	

Figure Number	Dataset/Code Name	Type	File Name/Specificities	License Type	Dataset/Code Citation	Dataset/Code URL	Related Publications
Figure 7.4 (continued)		Data	data_input/Marshall_et_al_2020_GRL data_input/Smith_et_al_ACP_2020 data_input/Smith_et_al_GRL_2018 data_input/Hodnebrog_et_al_2020_npj			https://github.com/IPCC-WG1/Chapter-7 (accessed 28/01/2022)	Smith et al. (2018b, 2020); Hodnebrog et al. (2020); Marshall et al. (2020)
Figure 7.5		Code	notebooks/060_chapter7_fig7.5_SPM_fig15.ipynb	MIT		https://github.com/IPCC-WG1/Chapter-7 (accessed 28/01/2022)	
		Data	data_input/Smith_et_al_ACP_2020			https://github.com/IPCC-WG1/Chapter-7 (accessed 28/01/2022)	Zelinka et al. (2014); Smith et al. (2020)
Figure 7.6		Code	notebooks/100_chapter7_fig7.6.ipynb	MIT		https://github.com/IPCC-WG1/Chapter-7 (accessed 28/01/2022)	
Figure 7.7		Code	notebooks/220_chapter7_fig7.7.ipynb	MIT		https://github.com/IPCC-WG1/Chapter-7 (accessed 28/01/2022)	
Figure 7.8		Code	notebooks/230_chapter7_fig7.8.ipynb	MIT		https://github.com/IPCC-WG1/Chapter-7 (accessed 28/01/2022)	
Cross-Chapter Box 7.1, Figure 7.1	Model datasets	Code	notebooks/box-71-figure-1/110_plot_box_7-1_emulator_overview_figure_projections_panels.ipynb	Nicholls et al. (2021)		https://gitlab.com/magicc/ar6-wg1-plots-and-processing	
		Data	All models below use historical and SSP1-2.6 ACCESS-CM2 r1i1p1f1 ACCESS-ESM1-5 r1i1p1f1 BCC-CSM2-MR r1i1p1f1 CESM2 r4i1p1f1 CESM2-WACCM r1i1p1f1 CMCC-CM2-SR5 r1i1p1f1 CNRM-CM6-1 r1i1p1f2 CNRM-CM6-1-HR r1i1p1f2 CNRM-ESM2-1 r1i1p1f2 CanESM5 r1i1p1f1 CanESM5-CanOE r1i1p2f1 FGOALS-g3 r1i1p1f1 GISS-E2-1-G r1i1p1f2 IPSL-CM6A-LR r1i1p1f2 MIROC-ES2L r1i1p1f2 MIROC6 r1i1p1f1 MPI-ESM1-2-LR r1i1p1f1 MRI-ESM2-0 r1i1p1f1 UKESM1-0-LL r4i1p1f2			https://esgf-node.llnl.gov/search/cmip6/ (accessed 28/01/2022)	

Figure Number	Dataset/Code Name	Type	File Name/Specificities	License Type	Dataset/Code Citation	Dataset/Code URL	Related Publications
Cross-Chapter Box 7.1, Figure 7.1 (continued)		Data	data/raw/fair/v20210211/scmdatabase/FairRv1.6.2 data/raw/cicero/2.0.1/scmdatabase/Cicero-SCM data/raw/magicc/v20210217/output_210_idealised_experiments_2021_02_17_230201/MAGICCv7.5.1 data/raw/oscar/v20210217/scmdatabase/OSCARv3.1.1			https://gitlab.com/magicc/ar6-wg1-plots-and-processing	Meinshausen et al. (2011a); Gasser et al., (2017a); Smith et al. (2018a); Nicholls et al. (2020)
Figure 7.10		Code	AR6_fbk_violin_plot.py	MIT	Zelinka (2021)	https://github.com/mzelinka/AR6_figure (accessed 28/01/2022)	
		Data	cmip56_feedbacks_AR6.json			https://github.com/mzelinka/AR6_figure (accessed 28/01/2022)	Zelinka et al. (2020)
Figure 7.11	Nonlinearity in alpha	Code	nonlin/nonlin_fgd.pro		Lunt (2021)	https://github.com/danlunt1976/ipcc_ar6 (accessed 28/01/2022)	
		Data					Models: Caballero and Huber (2013); Jonko et al. (2013); Meraner et al. (2013); Good et al. (2015); Duan et al. (2019); Mauritsen et al. (2019); Stolpe et al. (2019); Zhu et al. (2019) Proxies: von der Heydt et al. (2014); Anagnostou et al. (2016, 2020); Friedrich et al. (2016); Royer (2016); Shaffer et al. (2016); Köhler et al. (2017); Snyder (2019); Stap et al. (2019)
Figure 7.13	Paleo-polar amplification	Code	patterns/fgd/plot_all_fgd.pro		Lunt (2021)	https://github.com/danlunt1976/ipcc_ar6 (accessed 28/01/2022)	
		Data					Paleo models: Haywood et al. (2020); Zhu et al. (2020, 2021); Kageyama et al. (2021); Lunt et al. (2021); Zhang et al. (2021) Proxies: Bartlein et al. (2011); Salzmann et al. (2013); Vieira et al. (2018); Hollis et al. (2019); Cleator et al. (2020); McClymont et al. (2020); Tierney et al. (2020)
Figure 7.16		Code	notebooks/020_chapter7_fig7.16.ipynb	MIT		https://github.com/IPCC-WG1/Chapter-7 (accessed 28/01/2022)	
Figure 7.17		Code	contributed/fig7.17/tcr_fgd.f	MIT	[original author Masahiro Watanabe]	https://github.com/IPCC-WG1/Chapter-7 (accessed 28/01/2022)	
		Data					Geoffroy et al. (2013a); Smith et al. (2020)

Figure Number	Dataset/Code Name	Type	File Name/Specificities	License Type	Dataset/Code Citation	Dataset/Code URL	Related Publications
Figure 7.18		Code	notebooks/330_chapter7_fig7.18.ipynb	MIT	[original author Piers Forster]	https://github.com/IPCC-WG1/Chapter-7 (accessed 28/01/2022)	
		Data	data_input/Schlund_et_al_2020				Schlund et al. (2020)
Figure 7.19		Code	patterns/fgd/plot_all_fgd.pro		Lunt (2021)	https://github.com/danlunt1976/ipcc_ar6 (accessed 28/01/2022)	Haywood et al. (2020); Zhu et al. (2020, 2021); Kageyama et al. (2021); Lunt et al. (2021); Zhang et al. (2021)
		Data					
Figure 7.21		Code	notebooks/320_chapter7_fig7.21.ipynb	MIT	[original author William Collins]	https://github.com/IPCC-WG1/Chapter-7 (accessed 28/01/2022)	
		Data	data_input/fig7.20				
Figure 7.22		Code	notebooks/310_chapter7_fig7.22.ipynb	MIT	[original authors Piers Forster and Michelle Cain]	https://github.com/IPCC-WG1/Chapter-7 (accessed 28/01/2022)	
		Data					
FAQ 7.3, Figure 1	CDO commands and Python to plot the data points	Code	contributed/faq7.3_fig1	MIT	[original author Sophie Berger]	https://github.com/IPCC-WG1/Chapter-7 (accessed 28/01/2022)	
	Input is ECS for each model and projected 2081–2100 global warming in RCP8.5 and SSP5-8.5 respectively: 69 CMIP5 and CMIP6 model outputs.	Data	contributed/faq7.3_fig1				Schlund et al. (2020)

References

- Allen, R.J. et al., 2021: Significant climate benefits from near-term climate forcing mitigation in spite of aerosol reductions. *Environmental Research Letters*, **16**(3), 034010, doi:[10.1088/1748-9326/abe06b](https://doi.org/10.1088/1748-9326/abe06b).
- Anagnostou, E. et al., 2016: Changing atmospheric CO₂ concentration was the primary driver of early Cenozoic climate. *Nature*, **533**, 380–384, doi:[10.1038/nature17423](https://doi.org/10.1038/nature17423).
- Anagnostou, E. et al., 2020: Proxy evidence for state-dependence of climate sensitivity in the Eocene greenhouse. *Nature Communications*, **11**(1), 4436, doi:[10.1038/s41467-020-17887-x](https://doi.org/10.1038/s41467-020-17887-x).
- Arora, V.K. et al., 2020: Carbon-concentration and carbon-climate feedbacks in CMIP6 models and their comparison to CMIP5 models. *Biogeosciences*, **17**(16), 4173–4222, doi:[10.5194/bg-17-4173-2020](https://doi.org/10.5194/bg-17-4173-2020).
- Bartlein, P.J. et al., 2011: Pollen-based continental climate reconstructions at 6 and 21 ka: a global synthesis. *Climate Dynamics*, **37**(3), 775–802, doi:[10.1007/s00382-010-0904-1](https://doi.org/10.1007/s00382-010-0904-1).
- Caballero, R. and M. Huber, 2013: State-dependent climate sensitivity in past warm climates and its implications for future climate projections. *Proceedings of the National Academy of Sciences*, **110**(35), 14162–14167, doi:[10.1073/pnas.1303365110](https://doi.org/10.1073/pnas.1303365110).
- Checa-Garcia, R., M.I. Hegglin, D. Kinnison, D.A. Plummer, and K.P. Shine, 2018: Historical Tropospheric and Stratospheric Ozone Radiative Forcing Using the CMIP6 Database. *Geophysical Research Letters*, **45**(7), 3264–3273, doi:[10.1002/2017gl076770](https://doi.org/10.1002/2017gl076770).
- Cleator, S.F., S.P. Harrison, N.K. Nichols, I.C. Prentice, and I. Roulstone, 2020: A new multivariable benchmark for Last Glacial Maximum climate simulations. *Climate of the Past*, **16**(2), 699–712, doi:[10.5194/cp-16-699-2020](https://doi.org/10.5194/cp-16-699-2020).
- Collins, W.J. et al., 2017: AerChemMIP: Quantifying the effects of chemistry and aerosols in CMIP6. *Geoscientific Model Development*, **10**(2), 585–607, doi:[10.5194/gmd-10-585-2017](https://doi.org/10.5194/gmd-10-585-2017).
- Duan, L., L. Cao, and K. Caldeira, 2019: Estimating Contributions of Sea Ice and Land Snow to Climate Feedback. *Journal of Geophysical Research: Atmospheres*, **124**(1), 199–208, doi:[10.1029/2018jd029093](https://doi.org/10.1029/2018jd029093).
- Ettmanan, M., G. Myhre, E.J. Highwood, and K.P. Shine, 2016: Radiative forcing of carbon dioxide, methane, and nitrous oxide: A significant revision of the methane radiative forcing. *Geophysical Research Letters*, **43**(24), 12614–12623, doi:[10.1002/2016gl071930](https://doi.org/10.1002/2016gl071930).
- Eyring, V. et al., 2016: Overview of the Coupled Model Intercomparison Project Phase 6 (CMIP6) experimental design and organization. *Geoscientific Model Development*, **9**(5), 1937–1958, doi:[10.5194/gmd-9-1937-2016](https://doi.org/10.5194/gmd-9-1937-2016).
- Eyring, V. et al., 2020: Earth System Model Evaluation Tool (ESMValTool) v2.0 – An extended set of large-scale diagnostics for quasi-operational and comprehensive evaluation of Earth system models in CMIP. *Geoscientific Model Development*, **13**(7), 3383–3438, doi:[10.5194/gmd-13-3383-2020](https://doi.org/10.5194/gmd-13-3383-2020).
- Friedrich, T., A. Timmermann, M. Tigchelaar, O.E. Timm, and A. Ganopolski, 2016: Nonlinear climate sensitivity and its implications for future greenhouse warming. *Science Advances*, **2**(11), e1501923, doi:[10.1126/sciadv.1501923](https://doi.org/10.1126/sciadv.1501923).
- Gasser, T. et al., 2017a: The compact Earth system model OSCAR v2.2: Description and first results. *Geoscientific Model Development*, **10**(1), 271–319, doi:[10.5194/gmd-10-271-2017](https://doi.org/10.5194/gmd-10-271-2017).
- Gasser, T. et al., 2017b: Accounting for the climate–carbon feedback in emission metric. *Earth System Dynamics*, **8**(2), 235–253, doi:[10.5194/esd-8-235-2017](https://doi.org/10.5194/esd-8-235-2017).
- Geoffroy, O. et al., 2013a: Transient Climate Response in a Two-Layer Energy-Balance Model. Part II: Representation of the Efficacy of Deep-Ocean Heat Uptake and Validation for CMIP5 AOGCMs. *Journal of Climate*, **26**(6), 1859–1876, doi:[10.1175/jcli-d-12-00196.1](https://doi.org/10.1175/jcli-d-12-00196.1).
- Geoffroy, O. et al., 2013b: Transient Climate Response in a Two-Layer Energy-Balance Model. Part I: Analytical Solution and Parameter Calibration Using CMIP5 AOGCM Experiments. *Journal of Climate*, **26**(6), 1841–1857, doi:[10.1175/jcli-d-12-00195.1](https://doi.org/10.1175/jcli-d-12-00195.1).
- Ghan, S.J. et al., 2013: A simple model of global aerosol indirect effects. *Journal of Geophysical Research: Atmospheres*, **118**(12), 6688–6707, doi:[10.1002/jgrd.50567](https://doi.org/10.1002/jgrd.50567).
- Ghimire, B. et al., 2014: Global albedo change and radiative cooling from anthropogenic land cover change, 1700 to 2005 based on MODIS, land use harmonization, radiative kernels, and reanalysis. *Geophysical Research Letters*, **41**(24), 9087–9096, doi:[10.1002/2014gl061671](https://doi.org/10.1002/2014gl061671).
- Gidden, M.J. et al., 2019: Global emissions pathways under different socioeconomic scenarios for use in CMIP6: a dataset of harmonized emissions trajectories through the end of the century. *Geoscientific Model Development*, **12**(4), 1443–1475, doi:[10.5194/gmd-12-1443-2019](https://doi.org/10.5194/gmd-12-1443-2019).
- Good, P. et al., 2015: Nonlinear regional warming with increasing CO₂ concentrations. *Nature Climate Change*, **5**(2), 138–142, doi:[10.1038/nclimate2498](https://doi.org/10.1038/nclimate2498).
- Gregory, J.M., T. Andrews, and P. Good, 2015: The inconstancy of the transient climate response parameter under increasing CO₂. *Philosophical Transactions of the Royal Society A: Mathematical, Physical and Engineering Sciences*, **373**(2054), 20140417, doi:[10.1098/rsta.2014.0417](https://doi.org/10.1098/rsta.2014.0417).
- Gregory, J.M. et al., 2004: A new method for diagnosing radiative forcing and climate sensitivity. *Geophysical Research Letters*, **31**(3), L03205, doi:[10.1029/2003gl018747](https://doi.org/10.1029/2003gl018747).
- Haywood, A.M. et al., 2020: The Pliocene Model Intercomparison Project Phase 2: large-scale climate features and climate sensitivity. *Climate of the Past*, **16**(6), 2095–2123, doi:[10.5194/cp-16-2095-2020](https://doi.org/10.5194/cp-16-2095-2020).
- Hodnebrog, Ø. et al., 2020: The effect of rapid adjustments to halocarbons and N₂O on radiative forcing. *npj Climate and Atmospheric Science*, **3**(1), 43, doi:[10.1038/s41612-020-00150-x](https://doi.org/10.1038/s41612-020-00150-x).
- Hoesly, R.M. et al., 2018: Historical (1750–2014) anthropogenic emissions of reactive gases and aerosols from the Community Emissions Data System (CEDS). *Geoscientific Model Development*, **11**(1), 369–408, doi:[10.5194/gmd-11-369-2018](https://doi.org/10.5194/gmd-11-369-2018).
- Hollis, C.J. et al., 2019: The DeepMIP contribution to PMIP4: methodologies for selection, compilation and analysis of latest Paleocene and early Eocene climate proxy data, incorporating version 0.1 of the DeepMIP database. *Geoscientific Model Development*, **12**(7), 3149–3206, doi:[10.5194/gmd-12-3149-2019](https://doi.org/10.5194/gmd-12-3149-2019).
- Jiménez-de-la-Cuesta, D. and T. Mauritsen, 2019: Emergent constraints on Earth's transient and equilibrium response to doubled CO₂ from post-1970s global warming. *Nature Geoscience*, **12**(11), 902–905, doi:[10.1038/s41561-019-0463-y](https://doi.org/10.1038/s41561-019-0463-y).
- Jonko, A.K., K.M. Shell, B.M. Sanderson, and G. Danabasoglu, 2013: Climate Feedbacks in CCSM3 under Changing CO₂ Forcing. Part II: Variation of Climate Feedbacks and Sensitivity with Forcing. *Journal of Climate*, **26**(9), 2784–2795, doi:[10.1175/jcli-d-12-00479.1](https://doi.org/10.1175/jcli-d-12-00479.1).
- Joos, F. et al., 2013: Carbon dioxide and climate impulse response functions for the computation of greenhouse gas metrics: A multi-model analysis. *Atmospheric Chemistry and Physics*, **13**(5), 2793–2825, doi:[10.5194/acp-13-2793-2013](https://doi.org/10.5194/acp-13-2793-2013).
- Jungclaus, J.H. et al., 2017: The PMIP4 contribution to CMIP6 Part 3: The last millennium, scientific objective, and experimental design for PMIP4 simulations. *Geoscientific Model Development*, **10**(11), 4005–4033, doi:[10.5194/gmd-10-4005-2017](https://doi.org/10.5194/gmd-10-4005-2017).
- Kageyama, M. et al., 2021: The PMIP4 Last Glacial Maximum experiments: preliminary results and comparison with the PMIP3 simulations. *Climate of the Past*, **17**(3), 1065–1089, doi:[10.5194/cp-17-1065-2021](https://doi.org/10.5194/cp-17-1065-2021).

- Kanaya, Y. et al., 2020: Rapid reduction in black carbon emissions from China: Evidence from 2009–2019 observations on Fukue Island, Japan. *Atmospheric Chemistry and Physics*, **20**(11), 6339–6356, doi:[10.5194/acp-20-6339-2020](https://doi.org/10.5194/acp-20-6339-2020).
- Köhler, P. et al., 2017: A State-Dependent Quantification of Climate Sensitivity Based on Paleodata of the Last 2.1 Million Years. *Paleoceanography*, **32**(11), 1102–1114, doi:[10.1002/2017pa003190](https://doi.org/10.1002/2017pa003190).
- Kovilakam, M. et al., 2020: The Global Space-based Stratospheric Aerosol Climatology (version 2.0): 1979–2018. *Earth System Science Data*, **12**(4), 2607–2634, doi:[10.5194/essd-12-2607-2020](https://doi.org/10.5194/essd-12-2607-2020).
- Lauer, A. et al., 2020: Earth System Model Evaluation Tool (ESMValTool) v2.0 – Diagnostics for emergent constraints and future projections from Earth system models in CMIP. *Geoscientific Model Development*, **13**(9), 4205–4228, doi:[10.5194/gmd-13-4205-2020](https://doi.org/10.5194/gmd-13-4205-2020).
- Lee, D.S. et al., 2021: The contribution of global aviation to anthropogenic climate forcing for 2000 to 2018. *Atmospheric Environment*, **244**, 117834, doi:[10.1016/j.atmosenv.2020.117834](https://doi.org/10.1016/j.atmosenv.2020.117834).
- Loeb, N.G. et al., 2020: New Generation of Climate Models Track Recent Unprecedented Changes in Earth's Radiation Budget Observed by CERES. *Geophysical Research Letters*, **47**(5), e2019GL086705, doi:[10.1029/2019gl086705](https://doi.org/10.1029/2019gl086705).
- Lunt, D.J., 2021: Code and data for Chapter 7. GitHub. Retrieved from: https://github.com/danlunt1976/ipcc_ar6.
- Lunt, D.J. et al., 2021: DeepMIP: Model intercomparison of early Eocene climatic optimum (EECO) large-scale climate features and comparison with proxy data. *Climate of the Past*, **17**(1), 203–227, doi:[10.5194/cp-17-203-2021](https://doi.org/10.5194/cp-17-203-2021).
- Marshall, L.R. et al., 2020: Large Variations in Volcanic Aerosol Forcing Efficiency Due to Eruption Source Parameters and Rapid Adjustments. *Geophysical Research Letters*, **47**(19), e2020GL090241, doi:[10.1029/2020gl090241](https://doi.org/10.1029/2020gl090241).
- Matthes, K. et al., 2017: Solar forcing for CMIP6 (v3.2). *Geoscientific Model Development*, **10**(6), 2247–2302, doi:[10.5194/gmd-10-2247-2017](https://doi.org/10.5194/gmd-10-2247-2017).
- Mauritsen, T. et al., 2019: Developments in the MPI-M Earth System Model version 1.2 (MPI-ESM1.2) and Its Response to Increasing CO₂. *Journal of Advances in Modeling Earth Systems*, **11**(4), 998–1038, doi:[10.1029/2018ms001400](https://doi.org/10.1029/2018ms001400).
- McCliment, E.L. et al., 2020: Lessons from a high-CO₂ world: an ocean view from ~3 million years ago. *Climate of the Past*, **16**(4), 1599–1615, doi:[10.5194/cp-16-1599-2020](https://doi.org/10.5194/cp-16-1599-2020).
- Meehl, G.A. et al., 2020: Context for interpreting equilibrium climate sensitivity and transient climate response from the CMIP6 Earth system models. *Science Advances*, **6**(26), eaba1981, doi:[10.1126/sciadv.aba1981](https://doi.org/10.1126/sciadv.aba1981).
- Meinshausen, M., S.C.B.B. Raper, and T.M.L.L. Wigley, 2011a: Emulating coupled atmosphere-ocean and carbon cycle models with a simpler model, MAGICC6 – Part 1: Model description and calibration. *Atmospheric Chemistry and Physics*, **11**(4), 1417–1456, doi:[10.5194/acp-11-1417-2011](https://doi.org/10.5194/acp-11-1417-2011).
- Meinshausen, M. et al., 2011b: The RCP greenhouse gas concentrations and their extensions from 1765 to 2300. *Climatic Change*, **109**(1), 213–241, doi:[10.1007/s10584-011-0156-z](https://doi.org/10.1007/s10584-011-0156-z).
- Meinshausen, M. et al., 2017: Historical greenhouse gas concentrations for climate modelling (CMIP6). *Geoscientific Model Development*, **10**(5), 2057–2116, doi:[10.5194/gmd-10-2057-2017](https://doi.org/10.5194/gmd-10-2057-2017).
- Meinshausen, M. et al., 2020: The shared socio-economic pathway (SSP) greenhouse gas concentrations and their extensions to 2500. *Geoscientific Model Development*, **13**(8), 3571–3605, doi:[10.5194/gmd-13-3571-2020](https://doi.org/10.5194/gmd-13-3571-2020).
- Meraner, K., T. Mauritsen, and A. Voigt, 2013: Robust increase in equilibrium climate sensitivity under global warming. *Geophysical Research Letters*, **40**(22), 5944–5948, doi:[10.1002/2013gl058118](https://doi.org/10.1002/2013gl058118).
- Millar, R.J., Z.R. Nicholls, P. Friedlingstein, and M.R. Allen, 2017: A modified impulse-response representation of the global near-surface air temperature and atmospheric concentration response to carbon dioxide emissions. *Atmospheric Chemistry and Physics*, **17**(11), 7213–7228, doi:[10.5194/acp-17-7213-2017](https://doi.org/10.5194/acp-17-7213-2017).
- Myhre, G., E.J. Highwood, K.P. Shine, and F. Stordal, 1998: New estimates of radiative forcing due to well mixed greenhouse gases. *Geophysical Research Letters*, **25**(14), 2715–2718, doi:[10.1029/98gl01908](https://doi.org/10.1029/98gl01908).
- Myhre, G. et al., 2013a: Radiative forcing of the direct aerosol effect from AeroCom Phase II simulations. *Atmospheric Chemistry and Physics*, **13**(4), 1853–1877, doi:[10.5194/acp-13-1853-2013](https://doi.org/10.5194/acp-13-1853-2013).
- Myhre, G. et al., 2013b: Anthropogenic and Natural Radiative Forcing. In: *Climate Change 2013: The Physical Science Basis. Contribution of Working Group I to the Fifth Assessment Report of the Intergovernmental Panel on Climate Change* [Stocker, T.F., D. Qin, G.-K. Plattner, M. Tignor, S.K. Allen, J. Boschung, A. Nauels, Y. Xia, V. Bex, and P.M. Midgley (eds.)]. Cambridge University Press, Cambridge, United Kingdom and New York, NY, USA, pp. 659–740, doi:[10.1017/cbo9781107415324.018](https://doi.org/10.1017/cbo9781107415324.018).
- Newman, P.A., J.S. Daniel, D.W. Waugh, and E.R. Nash, 2007: A new formulation of equivalent effective stratospheric chlorine (EESC). *Atmospheric Chemistry and Physics*, **7**(17), 4537–4552, doi:[10.5194/acp-7-4537-2007](https://doi.org/10.5194/acp-7-4537-2007).
- Nicholls, Z.R.J. and J. Lewis, 2021: Reduced Complexity Model Intercomparison Project (RCMIP) protocol (v5.1.0). Zenodo. Retrieved from: https://doi.org/10.5281/zenodo.4589756#yh_83j7nmpu.mendeley.
- Nicholls, Z.R.J., J. Lewis, and M. Meinshausen, 2021: Code and data for Cross Chapter Box 7.1. GitLab. Retrieved from: <https://gitlab.com/magicc/ar6-wg1>.
- Nicholls, Z.R.J. et al., 2020: Reduced Complexity Model Intercomparison Project Phase 1: introduction and evaluation of global-mean temperature response. *Geoscientific Model Development*, **13**(11), 5175–5190, doi:[10.5194/gmd-13-5175-2020](https://doi.org/10.5194/gmd-13-5175-2020).
- Paulot, F., D. Paynter, P. Ginoux, V. Naik, and L.W. Horowitz, 2018: Changes in the aerosol direct radiative forcing from 2001 to 2015: Observational constraints and regional mechanisms. *Atmospheric Chemistry and Physics*, **18**(17), 13265–13281, doi:[10.5194/acp-18-13265-2018](https://doi.org/10.5194/acp-18-13265-2018).
- Riahi, K. et al., 2011: RCP 8.5 – A scenario of comparatively high greenhouse gas emissions. *Climatic Change*, **109**(1), 33–57, doi:[10.1007/s10584-011-0149-y](https://doi.org/10.1007/s10584-011-0149-y).
- Righi, M. et al., 2020: Earth System Model Evaluation Tool (ESMValTool) v2.0 – technical overview. *Geoscientific Model Development*, **13**(3), 1179–1199, doi:[10.5194/gmd-13-1179-2020](https://doi.org/10.5194/gmd-13-1179-2020).
- Royer, D.L., 2016: Climate Sensitivity in the Geologic Past. *Annual Review of Earth and Planetary Sciences*, **44**(1), 277–293, doi:[10.1146/annurev-earth-100815-024150](https://doi.org/10.1146/annurev-earth-100815-024150).
- Salzmann, U. et al., 2013: Challenges in quantifying Pliocene terrestrial warming revealed by data-model discord. *Nature Climate Change*, **3**(11), 969–974, doi:[10.1038/nclimate2008](https://doi.org/10.1038/nclimate2008).
- Schlund, M., A. Lauer, P. Gentine, S. Sherwood, and V. Eyring, 2020: Emergent constraints on Equilibrium Climate Sensitivity in CMIP5: do they hold for CMIP6? *Earth System Dynamics*, **11**, 1233–1258, doi:[10.5194/esd-11-1233-2020](https://doi.org/10.5194/esd-11-1233-2020).
- Shaffer, G., M. Huber, R. Rondanelli, and J.O. Pepke Pedersen, 2016: Deep time evidence for climate sensitivity increase with warming. *Geophysical Research Letters*, **43**(12), 6538–6545, doi:[10.1002/2016gl069243](https://doi.org/10.1002/2016gl069243).
- Sherwood, S.C., V. Dixit, and C. Salomez, 2018: The global warming potential of near-surface emitted water vapour. *Environmental Research Letters*, **13**(10), 104006, doi:[10.1088/1748-9326/aae018](https://doi.org/10.1088/1748-9326/aae018).
- Skeie, R.B. et al., 2020: Historical total ozone radiative forcing derived from CMIP6 simulations. *npj Climate and Atmospheric Science*, **3**(1), 32, doi:[10.1038/s41612-020-00131-0](https://doi.org/10.1038/s41612-020-00131-0).
- Smith, C.J. et al., 2018a: FAIR v1.3: a simple emissions-based impulse response and carbon cycle model. *Geoscientific Model Development*, **11**(6), 2273–2297, doi:[10.5194/gmd-11-2273-2018](https://doi.org/10.5194/gmd-11-2273-2018).
- Smith, C.J. et al., 2018b: Understanding Rapid Adjustments to Diverse Forcing Agents. *Geophysical Research Letters*, **45**(21), 12023–12031, doi:[10.1029/2018gl079826](https://doi.org/10.1029/2018gl079826).
- Smith, C.J. et al., 2020: Effective radiative forcing and adjustments in CMIP6 models. *Atmospheric Chemistry and Physics*, **20**(16), 9591–9618, doi:[10.5194/acp-20-9591-2020](https://doi.org/10.5194/acp-20-9591-2020).

- Smith, C.J. et al., 2021: Code and data for Chapter 7. Retrieved from: <https://github.com/chrisroadmap/ar6>.
- Snyder, C.W., 2019: Revised estimates of paleoclimate sensitivity over the past 800,000 years. *Climatic Change*, **156**(1), 121–138, doi:[10.1007/s10584-019-02536-0](https://doi.org/10.1007/s10584-019-02536-0).
- Stap, L.B., P. Köhler, and G. Lohmann, 2019: Including the efficacy of land ice changes in deriving climate sensitivity from paleodata. *Earth System Dynamics*, **10**(2), 333–345, doi:[10.5194/esd-10-333-2019](https://doi.org/10.5194/esd-10-333-2019).
- Sterner, E.O., D.J.A. Johansson, and C. Azar, 2014: Emission metrics and sea level rise. *Climatic Change*, **127**(2), 335–351, doi:[10.1007/s10584-014-1258-1](https://doi.org/10.1007/s10584-014-1258-1).
- Stevens, B., 2015: Rethinking the Lower Bound on Aerosol Radiative Forcing. *Journal of Climate*, **28**(12), 4794–4819, doi:[10.1175/jcli-d-14-00656.1](https://doi.org/10.1175/jcli-d-14-00656.1).
- Stevenson, D.S. et al., 2013: Tropospheric ozone changes, radiative forcing and attribution to emissions in the Atmospheric Chemistry and Climate Model Intercomparison Project (ACCMIP). *Atmospheric Chemistry and Physics*, **13**(6), 3063–3085, doi:[10.5194/acp-13-3063-2013](https://doi.org/10.5194/acp-13-3063-2013).
- Stolpe, M.B., I. Medhaug, U. Beyerle, and R. Knutti, 2019: Weak dependence of future global mean warming on the background climate state. *Climate Dynamics*, **53**(7), 5079–5099, doi:[10.1007/s00382-019-04849-3](https://doi.org/10.1007/s00382-019-04849-3).
- Thornhill, G.D. et al., 2021a: Climate-driven chemistry and aerosol feedbacks in CMIP6 Earth system models. *Atmospheric Chemistry and Physics*, **21**(2), 1105–1126, doi:[10.5194/acp-21-1105-2021](https://doi.org/10.5194/acp-21-1105-2021).
- Thornhill, G.D. et al., 2021b: Effective radiative forcing from emissions of reactive gases and aerosols – a multi-model comparison. *Atmospheric Chemistry and Physics*, **21**(2), 853–874, doi:[10.5194/acp-21-853-2021](https://doi.org/10.5194/acp-21-853-2021).
- Tierney, J.E. et al., 2020: Past climates inform our future. *Science*, **370**(6517), eaay3701, doi:[10.1126/science.aay3701](https://doi.org/10.1126/science.aay3701).
- Toohey, M. and M. Sigl, 2017: Volcanic stratospheric sulfur injections and aerosol optical depth from 500 BCE to 1900 CE. *Earth System Science Data*, **9**(2), 809–831, doi:[10.5194/essd-9-809-2017](https://doi.org/10.5194/essd-9-809-2017).
- Van Marle, M.J.E. et al., 2017: Historic global biomass burning emissions for CMIP6 (BB4CMIP) based on merging satellite observations with proxies and fire models (1750–2015). *Geoscientific Model Development*, **10**(9), 3329–3357, doi:[10.5194/gmd-10-3329-2017](https://doi.org/10.5194/gmd-10-3329-2017).
- Velders, G.J.M., D.W. Fahey, J.S. Daniel, S.O. Andersen, and M. McFarland, 2015: Future atmospheric abundances and climate forcings from scenarios of global and regional hydrofluorocarbon (HFC) emissions. *Atmospheric Environment*, **123**, 200–209, doi:[10.1016/j.atmosenv.2015.10.071](https://doi.org/10.1016/j.atmosenv.2015.10.071).
- Vieira, M., M.J. Pound, and D.I. Pereira, 2018: The late Pliocene palaeoenvironments and palaeoclimates of the western Iberian Atlantic margin from the Rio Maior flora. *Palaeogeography, Palaeoclimatology, Palaeoecology*, **495**, 245–258, doi:[10.1016/j.palaeo.2018.01.018](https://doi.org/10.1016/j.palaeo.2018.01.018).
- von der Heydt, A.S., H.A. Dijkstra, P. Köhler, and R. Wal, 2014: On the background state dependency of (palaeo) climate sensitivity. *Geophysical Research Letters*, **41**(2), 6484–6492, doi:[10.1002/2014gl061121](https://doi.org/10.1002/2014gl061121).
- Zelinka, M.D., 2021: IPCC AR6 Figure 7.10. Retrieved from: https://github.com/mzelinka/ar6_figure.
- Zelinka, M.D., T. Andrews, P.M. Forster, and K.E. Taylor, 2014: Quantifying components of aerosol-cloud-radiation interactions in climate models. *Journal of Geophysical Research: Atmospheres*, **119**(12), 7599–7615, doi:[10.1002/2014jd021710](https://doi.org/10.1002/2014jd021710).
- Zelinka, M.D. et al., 2020: Causes of higher climate sensitivity in CMIP6 models. *Geophysical Research Letters*, **46**, 2019GL085782, doi:[10.1029/2019gl085782](https://doi.org/10.1029/2019gl085782).
- Zhang, Z. et al., 2021: Mid-Pliocene Atlantic Meridional Overturning Circulation simulated in PlioMIP2. *Climate of the Past*, **17**(1), 529–543, doi:[10.5194/cp-17-529-2021](https://doi.org/10.5194/cp-17-529-2021).
- Zhu, J., C.J. Poulsen, and J.E. Tierney, 2019: Simulation of Eocene extreme warmth and high climate sensitivity through cloud feedbacks. *Science Advances*, **5**(9), eaax1874, doi:[10.1126/sciadv.aax1874](https://doi.org/10.1126/sciadv.aax1874).
- Zhu, J., C.J. Poulsen, and B.L. Otto-Bliesner, 2020: High climate sensitivity in CMIP6 model not supported by paleoclimate. *Nature Climate Change*, **10**(5), 378–379, doi:[10.1038/s41558-020-0764-6](https://doi.org/10.1038/s41558-020-0764-6).

